Investigating the role of vegetation in controlling chemical weathering

A Thesis

submitted to

Indian Institute of Science Education and Research Pune in partial fulfilment of the requirements for the M.Sc Degree Programme

by

Athul Suresh

IISER PUNE

Indian Institute of Science Education and Research Pune

Dr. Homi Bhabha Road,

Pashan, Pune 411008, INDIA.

April, 2024

Supervisor: Shreyas Managave

Athul Suresh

Certificate

This is to certify that this dissertation entitled “Investigating the role of vegetation in controlling landform” towards the partial fulfilment of the M.Sc degree programme at the Indian Institute of Science Education and Research, Pune represents study/work carried out by Athul Suresh at Indian Institute of Science Education and Research under the supervision of Shreyas Managave, Associate Professor, Department of Earth and Climate Science, during the academic year 2023-2024.

Dr. Shreyas Managave

Committee:

Dr. Shreyas Managave

Dr. Sudipta Sarkar

To my incredible parents and my brother,

Your love and encouragement have been my strength,

This thesis is a tribute to your unwavering support

Declaration

I hereby declare that the matter embodied in the report entitled “Investigating the role of vegetation in controlling chemical weathering ” are the results of the work carried out by me at the Department of Earth and Climate Science, Indian Institute of Science Education & Research (IISER) Pune, under the supervision of Dr. Shreyas Managave,and the same has not been submitted elsewhere for any other degree. Wherever others contribute, every effort is made to indicate this clearly, with due reference to the literature and acknowledgment of collaborative research and discussions.

Athul Suresh

Date: 17/04/2024

List of Tables

List of Figures

Abstract

Physical and chemical weathering controls the denudation rate and influence the landscape's evolution. Physical weathering disintegrates rocks into smaller fragments. Chemical weathering involves altering and breaking down minerals and rocks through chemical reactions with water, atmospheric gases, and various solutes. This process contributes to the formation of soil, sediments, and landforms and has significant implications for nutrient cycling, carbon dioxide sequestration, and the overall stability of ecosystems. The dynamic interaction between natural vegetation and the alteration of rocks and minerals is a relatively uncertain aspect of weathering. The primary objective of this research is to examine how vegetation impacts physical and chemical weathering processes and subsequently influences the evolution of the landscape. The Tamhini Ghat region in the Western Ghats of Maharashtra, and Ottathai region of Kannur district in Kerala India, are the study areas that offers diverse vegetation cover and a geological landscape. These locations presents a unique opportunity to investigate the role of vegetation in weathering due to its varied flora and similar climatic and geological conditions. The vegetation and monsoonal climate create an environment where vegetation can significantly influence weathering rates through organic exudates, root action, and the modulation of water flow. This study will provide insights into the interconnectedness of biological and geological systems. By collecting water samples from this region, we aim to explore how the interaction between vegetation and chemical weathering manifests in pH variation and cation flux. Slope and landforms will be used to assess the physical weathering.

Acknowledgments

I express my deepest gratitude to my supervisor, Dr. Shreyas Managave, for his invaluable guidance and mentorship. His expertise and encouragement have been instrumental in shaping this thesis.

I also thank Dr. Sudipta Sarkar for his expert advice and insights. A heartfelt thank you goes to the members of the Biogeochemistry lab - Sindhoora, Rauf, Sushanth, Mahi, Amrita, Asish, and Shashank - for being amazing lab members and for their valuable inputs and suggestions. I am grateful to my dear friends, Mehafus, Abhishek, Aby, and all others at IISER, for their unwavering support, laughter, and companionship throughout this academic journey. Special thanks to Rakesh for his assistance with the Ion Chromatography analysis. Also, I extend my heartfelt appreciation to Gayathri for her constant reminders of my responsibilities and unconditional love and support. Lastly, I thank my family for being there for everything.

Chapter 1 Introduction

1.1 Weathering: Types and agents

Weathering is pivotal in shaping Earth's surface and landscape evolution over a geologic time scale. Chemical, physical, and biological weathering are the significant types of weathering. The interplay between these mechanisms and their relationship with vegetation cover is essential in comprehending landscape dynamics. The formation of secondary minerals from primary minerals involves different mechanisms in which temperature, pressure, and precipitation play a vital role. Weathering agents include water, air, temperature the fluctuation, and atmospheric gases.

- Chemical weathering: It involves water, atmospheric gases, and organic acids, which will interact with the primary mineral surfaces to produce secondary minerals. Chemical processes like dissolution, hydration, oxidation, and hydrolysis are involved in the breaking down of rock. It is the fundamental driver of soil formation, nutrient cycling, and geochemical fluxes in terrestrial ecosystems.
- Physical weathering is breaking down rock into smaller fragments without chemical alteration. Physical forces such as temperature variation, frost action, pressure release, and abrasion contribute to weathering. Biological weathering: Abiotic factors contribute to physical and chemical weathering, wherein biological weathering introduces biotic components in which living organisms contribute to rock substrate degradation and alteration. Plant roots, burrowing organisms, lichen, mosses, and microbial communities are essential biological weathering agents.

1.2 Western Ghats & Monsoon

Western ghats are mountain ranges along the Indian peninsula's western coast and run north-south. It is one of the world's most crucial passive margin escarpments (Kale, 2009). This mountain range contributes considerably to shaping India's climate, where The side where the wind blows directly typically receives an average yearly rainfall of 380 centimeters.(Rao, 1976). The western ghats are known for their rich variety of floral and faunal communities. The vegetation types include tropical and evergreen forests, montane sholas, dry deciduous to scrub forests, and moist deciduous forests. It occupies an area of 129,037 km2 with 39 other subtypes of forests (Pullaiah, 2024). The drainage areas surrounding the Western Ghats escarpment show notable relief and rugged surface due to prolonged exposure and denudation.(Das et al., 2022). The Deccan plateau, located east of the mountain range, is one example of an elevated plateau that defines the Ghats.

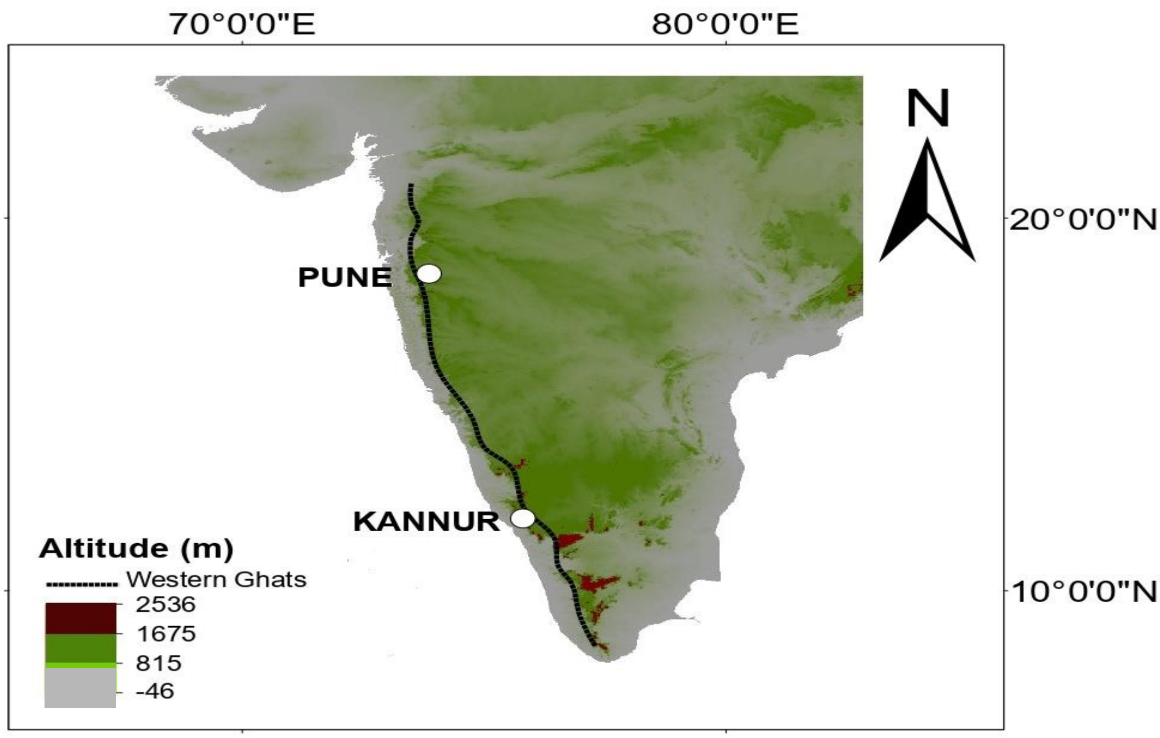

Figure 1.1 Western Ghats and altitude map of the western coast of India

The Indian subcontinent receives substantial annual rainfall due to the southwest monsoon. It makes up between 75 and 90 percent of the total precipitation(Mooley et al., 1981). Deccan plateau is shielded from southwest monsoon winds by western ghats. Through regional climate modifications, western ghat plays a crucial role in controlling the Indian climate (Gunnell, 1997). From June to September, the Indian west coast experiences heavy rainfall, including the southwest monsoon. During this period, all the water channels get filled, and the landscape modification rate through erosion and weathering increases. Also, the Ghat area has the highest vegetation cover, so this period can be a suitable time to study the vegetative control of chemical weathering using water chemistry.

1.3 The lithology of the sampling area

The Western Ghats stretch from Tamil Nadu in the south to the Satpura ranges in the north. In this stretch, Deccan basalt is the prominent rock type, covering a large area from the north to the middle of the Western Ghats. Other rock types present in this region include charnockite, granite, khondalite, gneiss, and limestone. The southern part of the Western Ghats has extensive laterite deposition. The sample collections for the current study were conducted in the Tamhini and Ottathai regions of Maharashtra and Kerala states, respectively. Tamhini ghat is located in the northern western ghats of Maharashtra. Mulshi Lake covers the study area's North, East, and South sides. The predominant lithology of this area is Deccan basalt. The Deccan Volcanic Province is a distinct large igneous province due to its volume (~2.5 × 106 km3), chronological proximity to the Cretaceous-Paleogene boundary (K-Pg boundary), and the compositional homogeneity of basaltic tholeiitic lavas which make up over 90% of its volume (Washington, 1922; West, 1958).

Nevertheless, in some areas of western India, undersaturated basalts, carbonatites, and nephelinites have also been found. Based on inter trappean sedimentary layers and ash beds, Deccan traps are divided into upper, middle, and lower. Also, on the basis of chemistry, it can be broadly categorized into upper and lower traps. The lower traps are found across the southern and eastern regions of the plateau., and the upper traps are present on the western coast of India. The low CaO, FeO, TiO_2 levels, Al_2O_3, and alkali concentrations distinguish the tholeiitic basalt from the upper and lower traps (Ghose, 1976). Major minerals present in the Deccan basalt include Olivine (Fo_{92} – Fo_{11}), pyroxene (augite to ferroaugite and pigeonite, spinel, ilmenite, feldspar (from An_{83} to albite, and anorthoclase to K-rich sanidine), and minor phases (amphibole, biotite, and pseudobrookite). Various mineral compositions indicate parental magma with differing levels of silica saturation (from slightly alkaline to tholeiitic). All tholeiitic magmas in Deccan consistently crystallize in low-pressure environments (Melluso & Sethna, 2011).

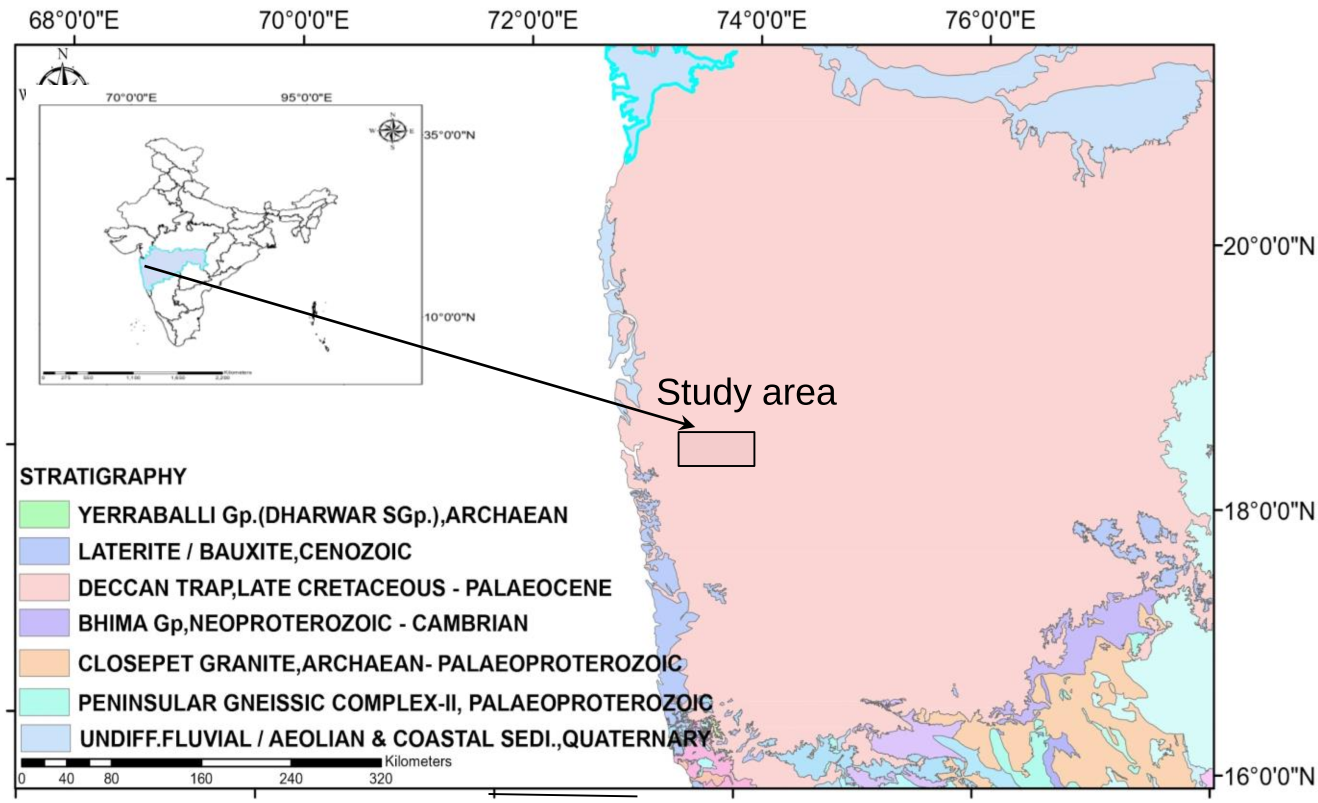

Fig 1.2 Map showing geology of the western part of Maharashtra, prepared in the GIS platform, shows various area litho-units (source: https://www.gsi.gov.in/webcenter/portal/OCBIS/pages_pageMAPS/pageMapsSeries).

The second study area, Ottathai, is located in the Kannur district of Kerala, which is close to the Kerala-Karnataka border. Unlike the northern part of western Ghat, which has the Deccan trap as its primary lithology, the southern part has diverse geology. Southernmost India's khondalite belt is a vast metasediments of granulite-facies likely of the early proterozoic age. The three primary types of rocks are charnockites (quartzofeldspathic gneisses with orthopyroxene), acid biotite-garnet graphitic gneisses, and migmatized khondalites (Chacko et al., 1987). The sampling area comprises charnockite composition. Charnockites occur in granulite terranes as orthopyroxene-bearing granitic orthogneiss (Rajesh & Santosh, 2012). This definition of charnockite has yet to be widely accepted by petrologists.

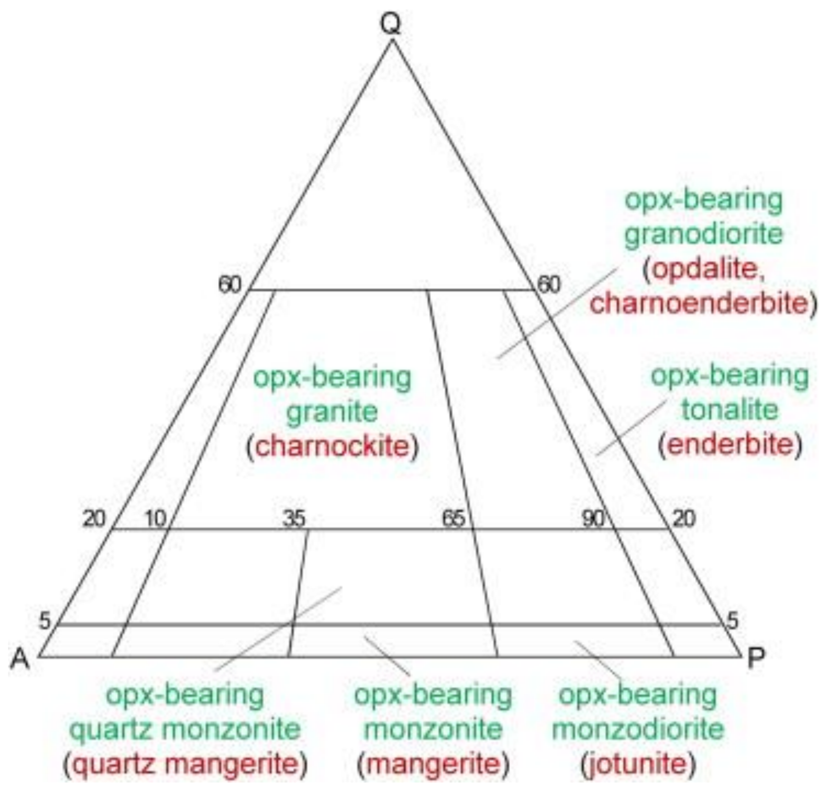

Fig 1.3 Quartz-alkali feldspar-plagioclase (QAP) diagram (Rajesh & Santosh, 2012)

Categorizing charnockite into igneous rocks or metamorphic rocks is a matter of debate. T.H Holland was the first person to define charnockite, and he defined charnockite as orthopyroxene-bearing granitic, igneous rock. According to (Cooray, 1969), south India's metamorphic rocks are metamorphic. They have complex foliation, are deeply stratified with different metasediments, and some even have garnet and graphite. Many have low K-feldspar content in which mineralogy corresponds to granodiorite or quartz monzonite rather than granite; in fact, most south indian rocks require tedious thin section analysis in order to show that some of them are, according to Hollands use, charnockite (Newton, 1992). These factors led to the widespread adoption of Pichamuthu's (1969) more inclusive and nongenetic interpretation of charnockite, which is any quartzofeldspathic rock containing orthopyroxene.

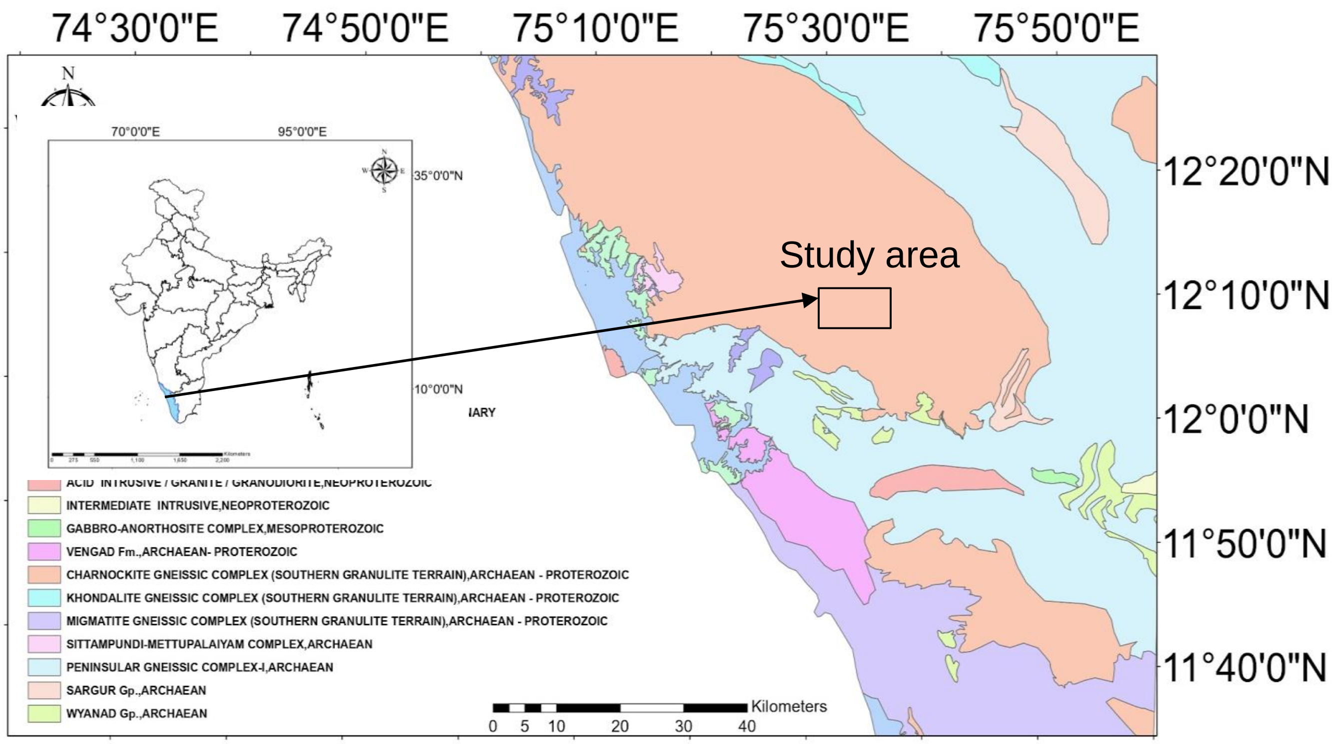

Fig. 1.4 Geological Map of the western part of Kannur, prepared in the GIS platform, shows various area litho-units (source: https://www.gsi.gov.in/webcenter/portal/OCBIS/pages_pageMAPS/pageMapsSeries).

The composition of orthopyroxene in charnockites varies from eulite En_{25} to hypersthene En_{64} (Subramaniam, 1959). According to Pichamuthu (1969), Indian charnockites contain orthopyroxene, clinopyroxene, hornblende, biotite, garnet, plagioclase, and potassium feldspar.

1.4 Factors controlling weathering

The two study areas have different geology, but the similar atmospheric conditions make them unique. The monsoon is the common factor between Kerala and Maharashtra. In the tropical climate, abundant precipitation occurs relatively more prolonged than in other regions; western ghats offer the same during monsoon. Comparatively long precipitation during this period helps to grow lush vegetation cover. Because of these climatic conditions, we can implement vegetation control on chemical weathering studies here.

Weathering rates strongly correlate with lithology (Garrels & MacKenzie, 1971; Meybeck, 1987; Bluth & Kump, 1994). Climatic conditions significantly affect weathering processes. Key factors include temperature, precipitation amount, runoff, and pH. Another important factor affecting the weathering rate of rock is the soil cover. A system covered by soil possesses hydrological and physical characteristics, such as residence time of water and high area of surface contact between water and minerals, which could significantly impact chemical weathering (Oliva et al., 2003). Studies on profiles of high soil cover (Stallard, 1985) were used to investigate the tropical river's low chemical weathering rate that drains the Amazonian plains and equatorial African region (Edmond et al., 1995; Gaillardet et al., 1995). Vegetation may act as a supporter of weathering and a suppressor of weathering. An environment with low-pH close to the root system, created by organic acid formed during plant biodegradation, improves mineral dissolution(Drever, 1994; HEYES, A.; MOORE et al.; Keeney, 2015). Also, vegetation cover can hold soil and form a thick cover over the parent rock to protect it from weathering. Below, the impact of several parameters affecting weathering is considered.

Weathering rates are strongly correlated with the lithology of the study area (Bluth & Kump, 1994). Research on how lithology affects weathering reveals that igneous and metamorphic rock that drains water is more acidic and diluted in significant cations than water-draining, more reactive lithologies, like serpentine (Krám et al., 1997), carbonates, and evaporites (Meybeck, 1987). The study areas are of charnockite and basaltic composition. The study on the clay fraction and its mineralogy of charnockite in the intermediate and wet zone of Srilanka is of biotite → vermiculite → halloysite → kaolinite order. In contrast, in the dry areas, smectite is present between vermiculite and halloysite (Cidu, 2001). Basalt weathering rises when annual mean temperature and precipitation rise (Sak et al., 2004). Studies on the clay mineral products of basalt weathering in the humid tropics have revealed that they differ significantly depending on environmental factors like rainfall, soil age, and drainage; however, the more advanced stages of weathering seem to produce more halloysite, kaolinite, gibbsite, goethite, and hematite (Evans, 1992; Nesbitt & Wilson, 1992; Sieffermann, G., & Millot, G, 1969). Temperature-related changes in weathering rates of silicate minerals like quartz and feldspar have been experimentally demonstrated (Blum & Stillings, 1995; Dove, 1995). When the temperature changes from 0 to 25 ℃, rate of weathering increase by an order of magnitude, according to the mean experimental activation energies of between 50 and 80 kJ/mol (White et al., 1999). A study by (White & Blum, 1995) suggests that temperature has the most considerable influence on chemical weathering, studies by (Millot et al., 2002) suggest that runoff has the highest influence. However, temperature and runoff are essential in determining the rate of weathering. Thermal expansion and contraction temperature induce physical weathering, and chemical reactions are accelerated at higher temperatures, so chemical weathering will also be higher. When precipitation rates are high, the availability of medium for chemical weathering gets higher, and the acidity of rainwater can affect rock mineralogy and alteration. Runoff of water facilitates the transport of dissolved ions and effectively contributes to chemical weathering. The residence period of minerals in the environment of weathering is longer than the reaction time when water and acid supply are greater than silicate minerals. This results in almost total alteration of the minerals before removal (West et al., 2005).

Plants and microbiota they are associated with can directly impact the chemical environment of minerals. For example, they produce organic acids, which can reduce pH, introduce organic chelates, and speed up weathering. They can also produce CO_2, through which pH can be reduced (Drever, 1994). The significance of pH studied by (Drever, 1994) states that most silicate minerals dissolve at different rates, depending on the pH in the circumneutral region; they dissolve more quickly when the pH in the acidic zone decreases and more quickly when the acidity in the alkaline region increases (Fig. 1.5).

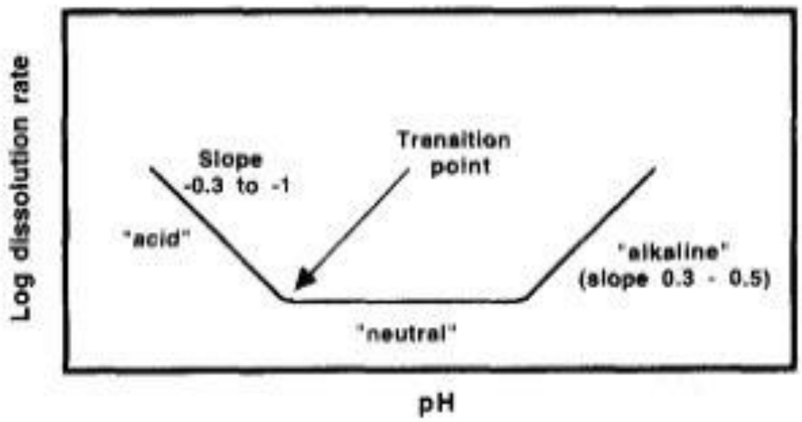

Fig. 1.5 Diagram showing the correlation between silicate mineral dissolving rate and pH (Drever, 1994)

If the primary cation source for weathering is alkali feldspar and intermediate plagioclases, then the transition pH will be approximately 4.5, and the rate of weathering will increase (Stumm, 1967). According to the studies done by Drever for Ca and Mg, the transition pH can be higher. More clarity in the literature regarding how organic ligands affect mineral weathering must be provided. There are sources of confusion: In certain studies, the pH needed to be buffered, making it impossible to distinguish between the pH and ligand effects clearly (Huang & Keller, 1970; MANLEY & EVANS, 1986).

1.5 Remote Sensing

Simply put, remote sensing is gathering data about an object without physically touching it. For studies that require temporal and spatial data of a much larger scale, data sets from satellites are used. Therefore, the term Remote sensing now refers to collecting electromagnetic radiation data (often with a wavelength range of 0.4 to 30cm) from sensors located on aerial or space platforms and interpreting that data to determine the characteristics of ground objects. The fundamental idea behind remote sensing is that different types of objects reflect or emit radiation at different wavelengths in the electromagnetic spectrum, depending on the composition or physical characteristics of the object (Gupta, 2017) (Fig. 1.6).

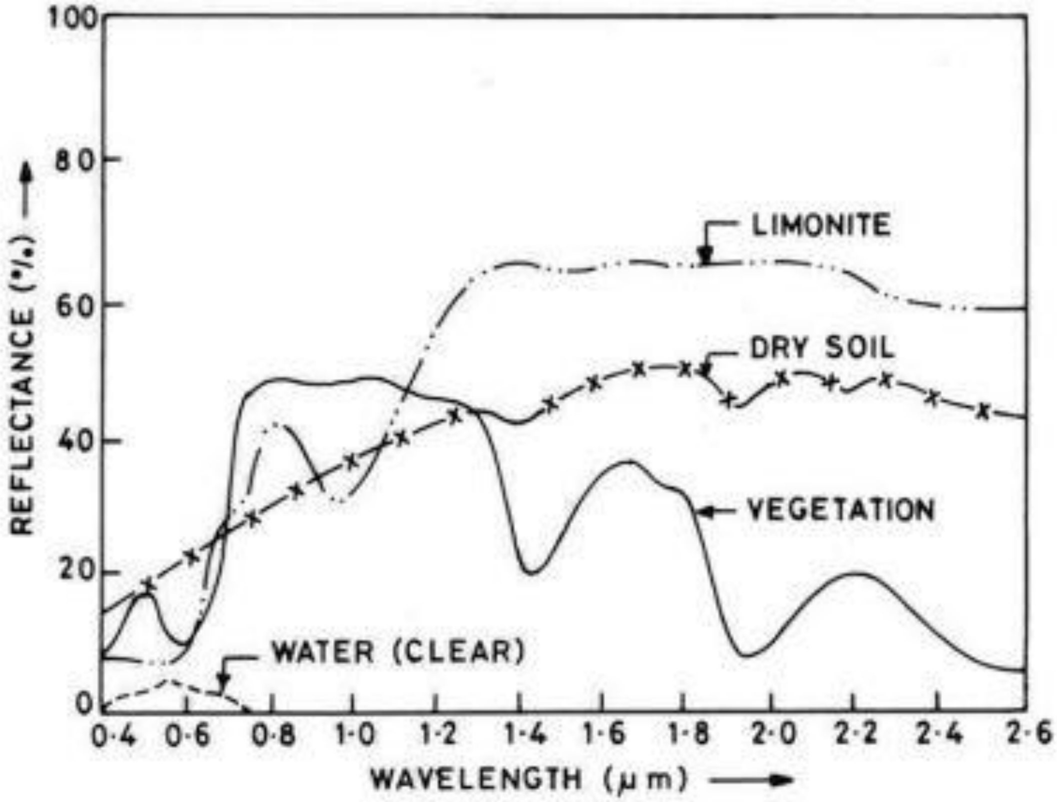

Fig. 1.6 Spatial reflectance curve of a few natural objects (Gupta, 2017).

A remote sensing mission's fundamental design requires understanding the spectral response curves, which display the strength of radiation produced or reflected by objects at various wavelengths.

In the proposed study, with the help of remote sensing principles, visualization and interpretation of the topographical features like altitude, slope, and aspect have been done. For NDVI and forest cover data, satellite datasets have been used and resampled to similar resolutions.

1.6 About this study

The Western Ghats are known for their abundance of varied flora and fauna and similar climatic conditions. This type of climatic condition is vital for the abundance of vegetation, hence, their control of weathering and landscape evolution. In the North and South of Western Ghat, the geology and the type of tree cover are different. By studying the Ion flux of the water collected from the study areas and correlating it with the annual mean forest cover data, we aim to examine the type of relationship between between the mentioned parameters. The slope is another critical parameter that can affect the weathering rate, so the role of slope in the weathering is also studied. Examining the correlation between ion concentrations and tree cover data can give insights into whether the weathering is supply-limited or supply-unlimited. The soil cover above the parent rock can affect the weathering. Trees can hold the soil and make a supply-limited weathering system. We need similar climatic conditions to study vegetation control on a lengthy hill range profile like the Western Ghats. Otherwise, different climatic conditions may affect the parameters' role in weathering. To some extent, that barrier of varied climatic conditions is not there in western Ghat because of monsoons.

The study on Amazon rainforests done by researchers ("Geochemistry of the Amazon: 3. Weathering Chemistry and Limits to Dissolved Inputs," 1987) found that thick soil cover development under transport-limited conditions caused the low weathering rate of parent rock in that region. In this study, we aim to investigate the controlling parameter of Western Ghats. This study can probably give insights into weathering and the controls of weathering in subtropical regions like the Western Ghats.

Chapter 2 Materials and Methods

2.1 Sample collection

Water samples for this study were collected from both the northern and southern regions of the Western Ghats. Specifically, the Tamhini Ghat, situated within the Pune-Raigad districts of Maharashtra state, served as the collection site for 14 water samples, thus representing the northern sector of the Western Ghats. Conversely, for the representative sample of the southern sector of the Western Ghats, the Ottathai region in the Kannur district of Kerala was selected as the collection site. One liter of water samples was collected from the field in a polyethylene bottle thoroughly rinsed with Milli-Q water. The water samples were obtained from flowing channels with minimal human contact. pH and temperature measurements of the samples were conducted onsite utilizing the HI98129 model pH instrument manufactured by Hanna Instruments. Calibration of the pH meter was done using various buffers, and its accuracy was verified multiple times. The instrument possesses an accuracy of 0.5℃ (1.0℉) for temperature measurements and 0.01 pH readings. Careful measures were taken during sample collection to prevent any contamination.

In the Tamhini study area, we selected fourteen watersheds based on their respective facing directions: five facing east, four facing north, three facing south, and two facing west, for sample collection. Samples were collected during two monsoon seasons, specifically in 2022 and 2023. The 2023 sample collection was done in three different months of the same monsoon period: July, August, and September, respectively.

In the Ottathai study area of Kerala, we identified eight sampling areas, considering three facing south, two facing east, two facing west, and one facing north. Sampling in this study area was conducted during the 2023 monsoon season. The longitude and latitude of all the sampling points are given below.

Name	Latitude	Longitude
N1	18.515686	73.465763
W1	18.518368	73.471236
E1	18.512363	73.481881
U1/E4	18.51159	73.48232
U2/E5	18.51095	73.48274
U3/N2	18.5103	73.48855
E2	18.50196	73.49772
E3	18.4976	73.49552
S1	18.49061	73.48479
U4/S2	18.49076	73.47772
U5/W2	18.48821	73.455
U6/S3	18.4964	73.43824
N5	18.4755	73.48788
N0	18.516	73.44608

Table 2.1 Latitude and longitude of Tamhini sampling locations

Name	Latitude	longitude
loc 1	12.197245	75.475181
loc 2	12.197046	75.484791
loc 3	12.196968	75.488305
loc 4	12.2	75.499
loc 5	12.2	75.496
loc 6	12.19971	75.494366
loc 7	12.219	75.484
loc 8	12.218	75.482

Table 2.2 Latitude and longitude of Ottathai sampling locations

2.2 Sample processing

The water samples taken from the field are carefully processed without causing any type of contamination. The samples are filtered using 0.2 µm Nylon membrane filter paper by vacuum filtration. 60 ml of each sample is treated with mercury chloride, collected in an amber bottle, and stored in the refrigerator and will be used for δ13C concentrations. The remaining filtered sample was divided equally and stored in two 500 ml Polyethylene bottles for cation and anion analysis. 2 ml of Nitric acid was added to one of them and used for cation analysis for pH adjustment and ionization of samples. Then, the samples were taken to measure the cation and anion concentrations using Ion Chromatography (IC) (Fig 2.1).

2.3 Cation & Anion Analysis using Ion Chromatography (IC)

Ion Chromatography was used to measure the concentrations of major cations and anions in the water samples. The significant cations include Ca^{2+}, Mg^{2+}, Na^{+}, and K^{+}. Furthermore, the anions considered for the study were Cl^{-}, NO_3^{-}, and SO_4^{2-}. The Instrument 882 Compact IC Plus is a type of instrument made by Metrohm Company, which is part of the Compact IC Plus series. It is a differential partitioning of ion-based techniques for separating mobile and stationary phases. A polymer or resin with ion exchange functional groups usually serves as the stationary phase. The mobile phase is the liquid that moves the sample through the column and elutes the separated ions. Cations and anions have different eluent or mobile phases. For anion, the solution of Na_2CO_3 and $NaHCO_3$ was used as the mobile phase or eluent. The mobile phase solution for cation constitutes dipicolinic acid ($C_7H_5NO_4$) and nitric acid (HNO_3). The interaction between the ions in the sample and the stationary phase occurs in the ion chromatography column based on their size and charge when injected. The ions with lesser affinity are eluted quicker from the column, while those with a greater affinity for the stationary phase are retained longer and eluted later. In the case of anion, fluorides are eluded earlier, followed by chlorides, nitrates, phosphates, and sulfate, respectively. For cations, sodium is eluded first, followed by potassium, calcium, and magnesium at the end.

Fig. 2.1 Methrom 882 compact IC Plus

The ions, once separated, are detected by a conductivity detector, which produces a signal proportional to the quantity of each ion eluted from the column. The detector used in Metrohm ion chromatography is a conductivity detector, which assesses the conductivity of the eluent as ions traverse through it. 1 ml of water sample is taken and diluted ten times before running in the instrument. The vials are cleaned five times using Milli-Q before and after use.

Eluent preparation for cation and anion

The eluent for cation concentration analysis is added 0.70 mM of dipicolinic acid and two mM of nitric acid in two liters of Milli-Q. The eluent was then filtered through 0.45 µm nylon filter paper. The column in the instrument is very sensitive, so ultrasonication of the eluent also needs to be done. This can remove the air bubbles in the eluent. Before every analysis, the eluent was freshly made because storing it for an extended period could cause changes to its characteristics.

In the case of anion, the eluent is made by adding 3.2 mM of Na_2CO_3 and 1 mM of $NaHCO_3$ in two liters of Milli-Q. After that, it was filtered using 0.45 µm nylon filter paper. Ultrasonication, as done in cation eluent, was also done for this eluent. An acid solution was also made for anion analysis along with the eluent. For IC column regeneration, 0.2 M concentration of H2SO4 was utilized. The acid solution was diluted and made to 200 milli mole and used to run the instrument. In anion analysis, the eluent contains bicarbonate and sodium ions, which exhibit high conductivity.

Meanwhile, the conductivity of sodium and anions in the sample is less. To address this issue, a process known as suppression is employed. During suppression, cations are exchanged with hydrogen ions, reducing the background signals of the mobile phase and increasing the signals of the ions intended for measurement. This technique helps improve the analysis's accuracy and sensitivity by minimizing interference from high-conductivity species and enhancing the detection of the target ions.

Standards preparation

The following equation was used to generate standard solutions of combined fluoride, chloride, nitrate, phosphate, and sulfate (anions). The same equation was used to generate standard solutions of combined sodium, potassium, calcium, and magnesium (cations) at concentrations of 0.1 µM, 0.25 µM, 0.5 µM, 1 µM, 2 µM, 4 µM and 6 µM from a stock solution of 50 µM:

$$N_1V_1 = N_2V_2$$

N and V stand for the volume and normality of the solutions, respectively. Each standard will have an area as the conductivity and retention time plot output. The standard curve equation of standards (area vs. concentration) was used to compute the sample concentration. Anion and cation concentration is expressed in µM/L and is computed using the standard curve.

2.4 Dissolved silica concentration using spectrophotometer

Water samples for the silica analysis were collected in clean polythene bottles. The filtered samples were collected in a non-glass container. Silicon and its derivatives, such as silica (SiO_2) and silicates (SiO_4^- or SiO_3^{2-}), are abundant in water. Furthermore, there are two forms of silica: silicate and silicic acid. In a spectrophotometer, the sample was treated with chemical agents like ammonium molybdate for the dissolved silica analysis. The yellow silico-molybdate complex is created when the silica composite combines with acidic ammonium molybdate and is reduced with sodium sulfite to produce a blue molybdate color. This is then measured in a 1 cm cell using a spectrophotometer set at 700 nm to compare to a standard of known concentration.

Reagents used

1. Hydrochloric acid, 0.25N
2. Ammonium molybdate, 5%
3. Disodium EDTA, 1%
4. Sodium sulfite, 17%
5. Silica standards

Working principle of spectrophotometer

The double-beam spectrophotometer works based on how light behaves when reflected and transmitted. It has a light source that emits intense beams of light, either ultraviolet and visible rays or infrared rays, depending on what is needed. The monochromator picks out light of a specific wavelength we want to analyze. This wavelength is chosen based on how the substance we are testing absorbs light. In the spectrophotometer, light from the source hits the sample, usually in a transparent container called a cuvette. If the sample is a liquid, it is placed in this cuvette. After passing through the sample, the remaining light hits a detector, turning it into an electrical signal. A computer then processes this signal.

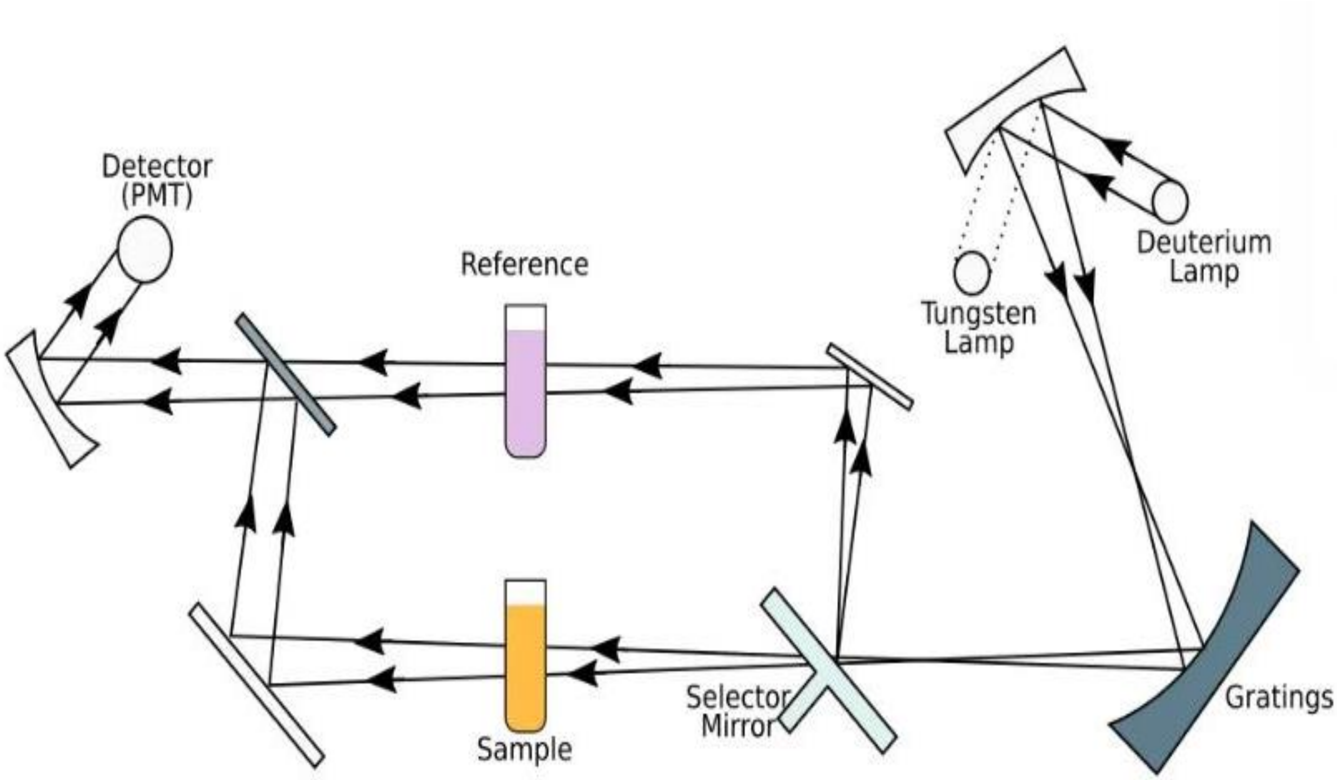

Fig. 2.2 Working of a spectrophotometer (source:www.smacgigworld.com)

In simpler terms, the spectrophotometer shines light through a sample, picks out specific light colors, and measures how much of that light gets absorbed by the sample. Then, it turns that information into an electrical signal that a computer can understand (Fig. 2.2). Spectrophotometry is the method used by a spectrophotometer to determine the amount of light absorbed by any chemical substance when a light beam passes through it. The instrument works based on the Beer-Lambert law. The amount of light absorbed has a linear relationship with the length of light and concentration of the sample.

$$A \propto C.L$$

In the above equation, A is the absorbance value, and C is the sample concentration. L is the path length.

$$A = -\log(T)$$

T is transmittance; It is a function of light passing through the sample

$$T = [\, I_T / I_0 \,]$$

I_T is the transmitted light, and I_0 is the incident light.

2.5 Study using Remote Sensing

The study area in Tamhini encompasses 14 distinct watersheds, while Ottathai comprises 8. With the help of Geographic Information System (GIS) software tools such as QGIS and ArcGIS, we delineated these watersheds to create maps. Subsequently, utilizing the same software, we analyzed the watershed characteristics, including slope, altitude, and aspect, to better understand their topographical features (Fig. 2.3). The NDVI data for two different months (April and November) was extracted from the sentinel-2 satellite imagery.

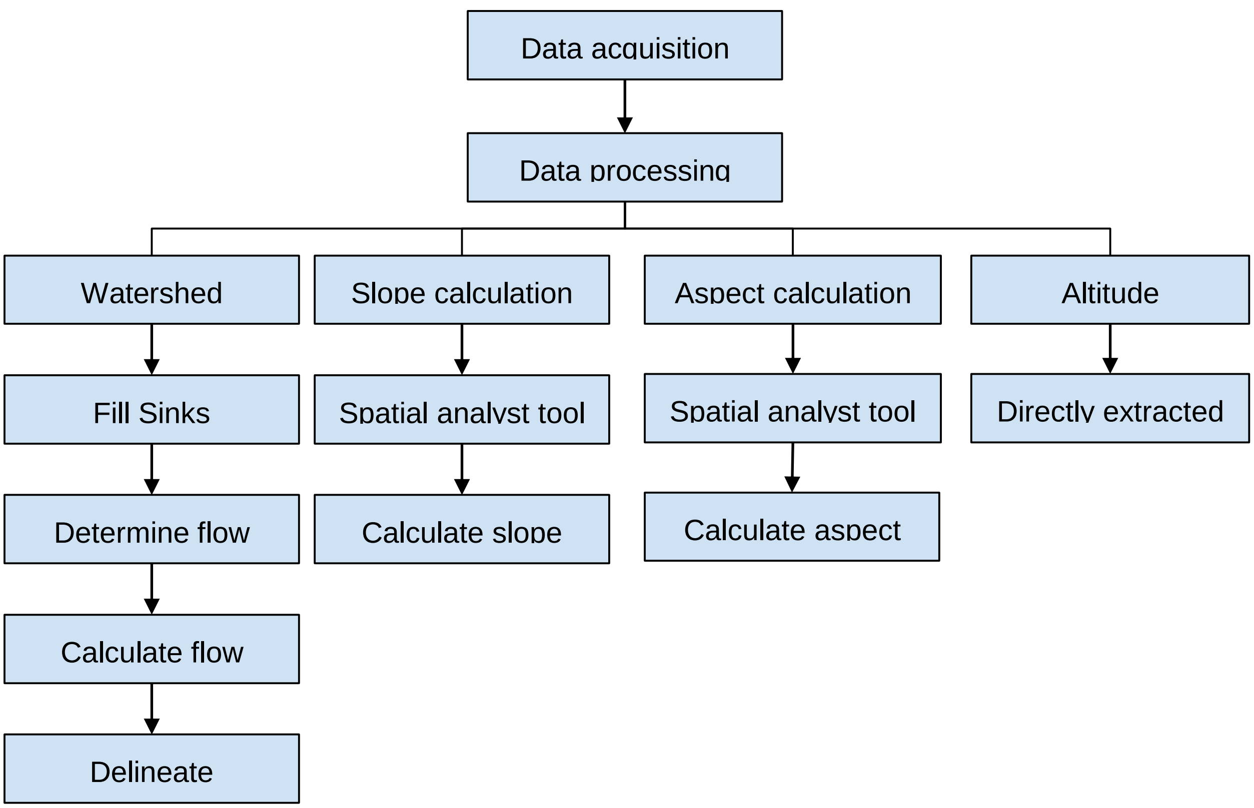

Fig. 2.3 Flow chart of the methodology used for DEM-based analysis

The DEM (Digital Elevation Model) from the SRTM (Shuttle Radar Topography Mission) database was used to calculate altitude, slope, and aspect and delineate the watershed. The hydrology tool of ArcGIS software was used for watershed delineation. To outline watersheds using a Digital Elevation Model (DEM), we have calculated the direction of water flow and then applied this information to the Watershed tool. Before determining the contributing area, we created a raster using the flow direction tool to show the flow direction. A flow accumulation threshold is then used to define a watershed, which means that the pour points for the watershed will be located at the junctions of a stream network obtained from flow accumulation. After doing all the above operations, we made a raster file of the watershed.

In order to verify the data created with the software, a toposheet map of the 1:50,000 scale provided by Survey of India was used. The watershed boundaries were carefully confirmed by aligning the toposheet map with the study area. Two toposheet maps were used for the study area Tamhini: 47F/7 and 47F/6. For the Ottathai sampling location in Kerala, 48P/12 was used.

A spatial analyst tool was used to measure slope and aspect. The Spatial Analyst toolbox offers a range of tools for analyzing and modeling spatial data, including raster (cell-based) and feature (vector) data types. The slope operation here was done to calculate the slope of the study area. The aspects were determined by performing aspect operations in the listed toolsets.

The data set published by (Hansen et al., 2013) was used for the tree cover data. The satellite image containing a specific band labeled "treecover2000" was utilized to extract tree cover data. Within this band, vegetation exceeding a height of 5 meters was included. Also, the DEM and the Hansen datasets share a similar resolution. The Hansen dataset has a resolution of 30 meters, similar to that of the DEM dataset. However, to minimize potential errors, the tree cover data was resampled to match the resolution of the DEM dataset (Fig. 2.4).

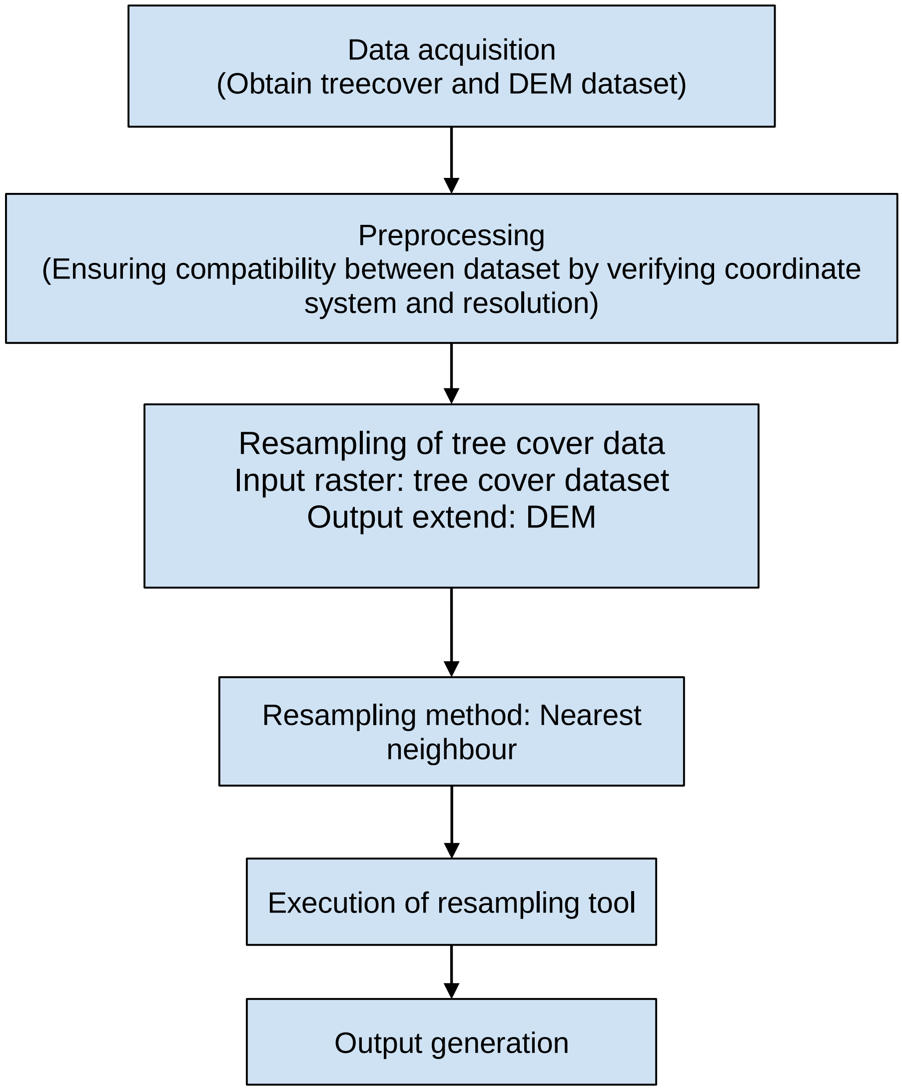

Fig. 2.4 Flow chart of the methodology used for Resampling of Hansen tree cover data

Along with the slope, aspect, altitude, and tree cover data, NDVI data for April and November was also extracted from the sentinel satellite image. NDVI, or Normalised Difference Vegetation Index, is an index of total vegetation cover in an area. The NDVI formula, derived from the red and near-infrared reflectance ratio (NDVI=(NIR-RED)/(NIR+RED)), calculates the ratio of near-infrared (NIR) to red (RED) light reflected by vegetation and captured by the satellite sensor (Fig. 2.5). This ratio is based on the principle that chlorophyll absorbs red light. At the same time, the leaf structure scatters near-infrared light. NDVI values vary between -1 and 1, where negative values indicate the absence of vegetation (Myneni et al., 1995; Running, 1990).

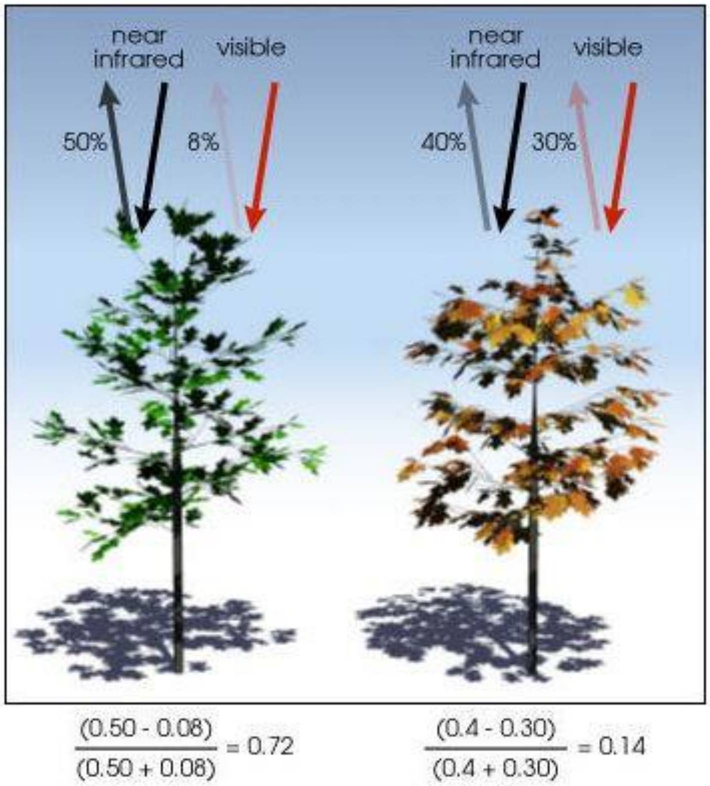

Fig. 2.5 NDVI (Source: NASA)

For Sentinel-2, the NIR band is B8, and the RED band is B4. So, the NDVI calculation equation for the sentinel data set will be,

$$NDVI := \ Index\ (B8, B4) \ = \frac{B8 - B4}{B8 + B4}$$

The slope, aspect, altitude, and NDVI were calculated for every watershed, alongside pixel-wise data extraction. Some datasets, such as the DEM and Sentinel satellite imagery, were observed to have different coordinate systems. In order to correlate data from these different sources, a reprojection operation was performed, aligning the coordinate systems of the datasets to reduce the associated errors. Slope, aspect, tree cover, altitude, and NDVI values were extracted for every pixel in the watershed (Fig. 2.6)

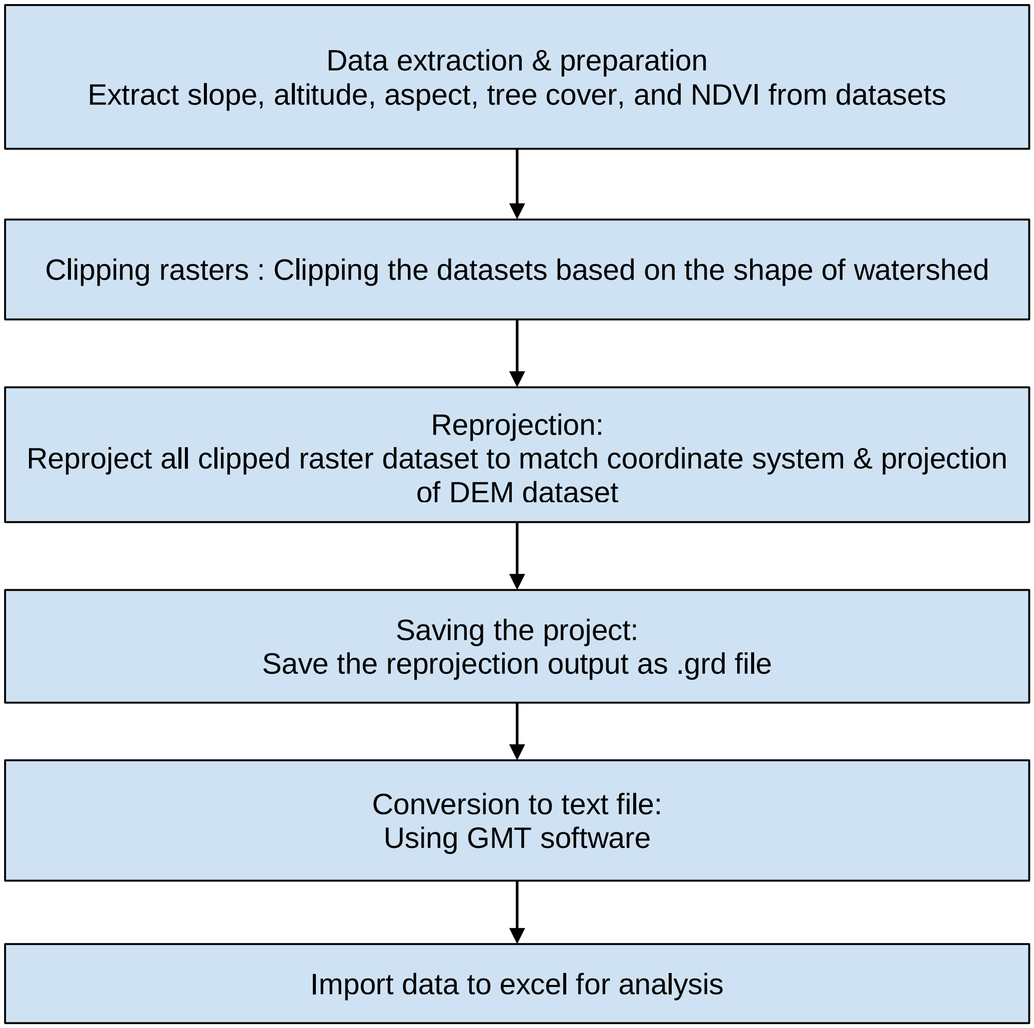

Fig. 2.6 Flow chart of the methodology used for the pixel-wise data extraction from shapefiles

The study areas (watershed) were clipped based on their area before the reprojection. The coordinate systems and projections of the reprojected dataset were closely observed and confirmed to have the same coordinate system. The project was saved in the .grd format. The ".grd" files comprise scalar data values organized in a consistent rectangular grid, positioned within (x, y) or (longitude, latitude) coordinates. The saved project was subsequently transformed into a text file using GMT (Generic Mapping Tools) software. Subsequently, the text files were imported into Microsoft Excel for further analysis.

Chapter 3 Results and Discussion

3.1 Topographical analysis

The topography of a region plays a crucial role in understanding its geological composition, landforms, and environmental characteristics. This section presents a detailed analysis of the topography of the Tamhini Ghat and Ottathai study regions, focusing on geology, altitude, slope, aspect, forest cover, and watershed analysis. The Deccan basaltic formations dominate the geology of Tamhini, and the Ottathai region of Kerala has a charnockite-dominated formation. Contour maps were used to study the altitude and the preliminary study for the possible drainage patterns in the watershed (Fig.3.1 & 3.2).

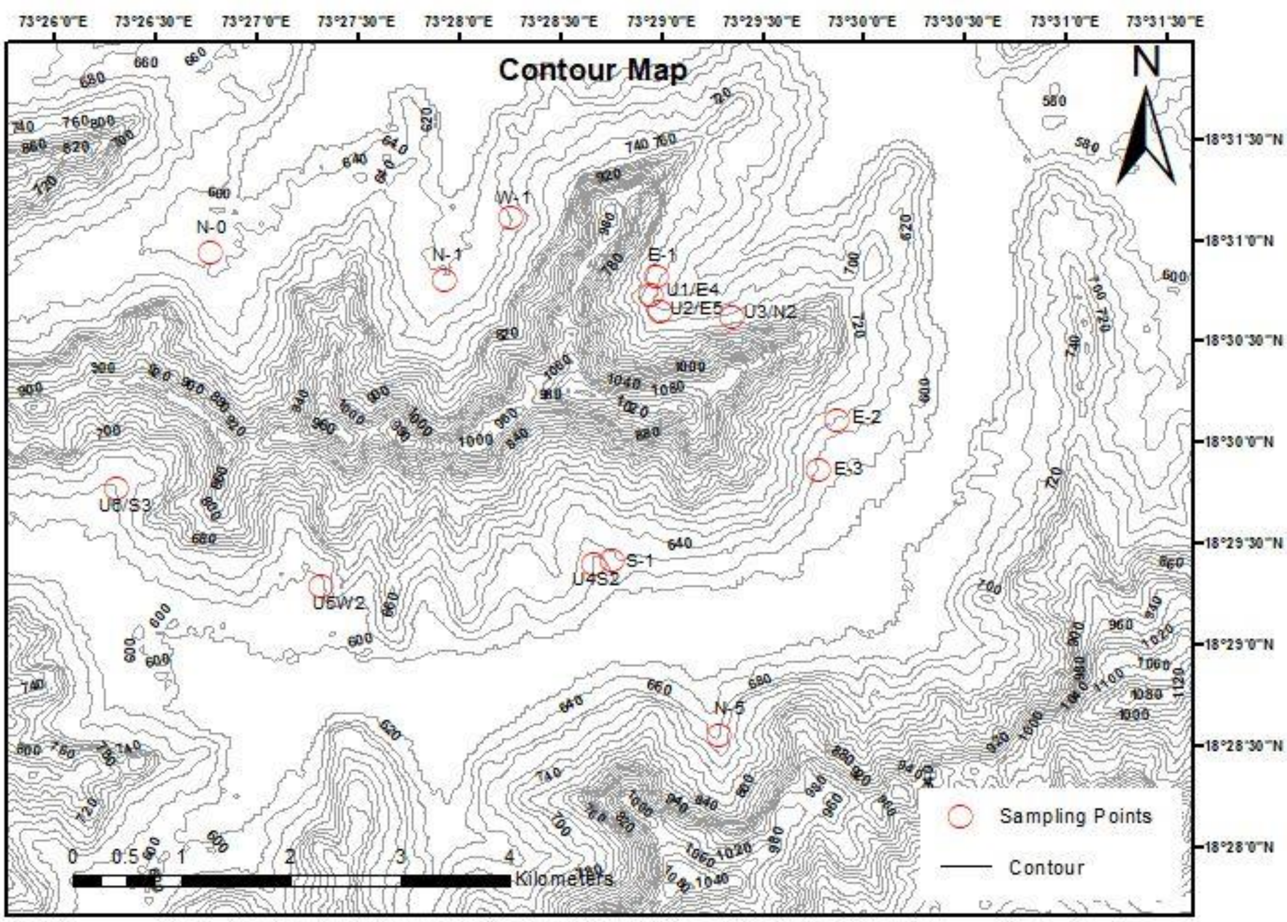

Fig. 3.1 Contour map of Tamhini study area

The highest elevation of this study area is 1080m, and the contour lines were placed at a distance of 10m from each other. Contour maps of the second study region were also made, and elevation and possible drainage areas were checked.

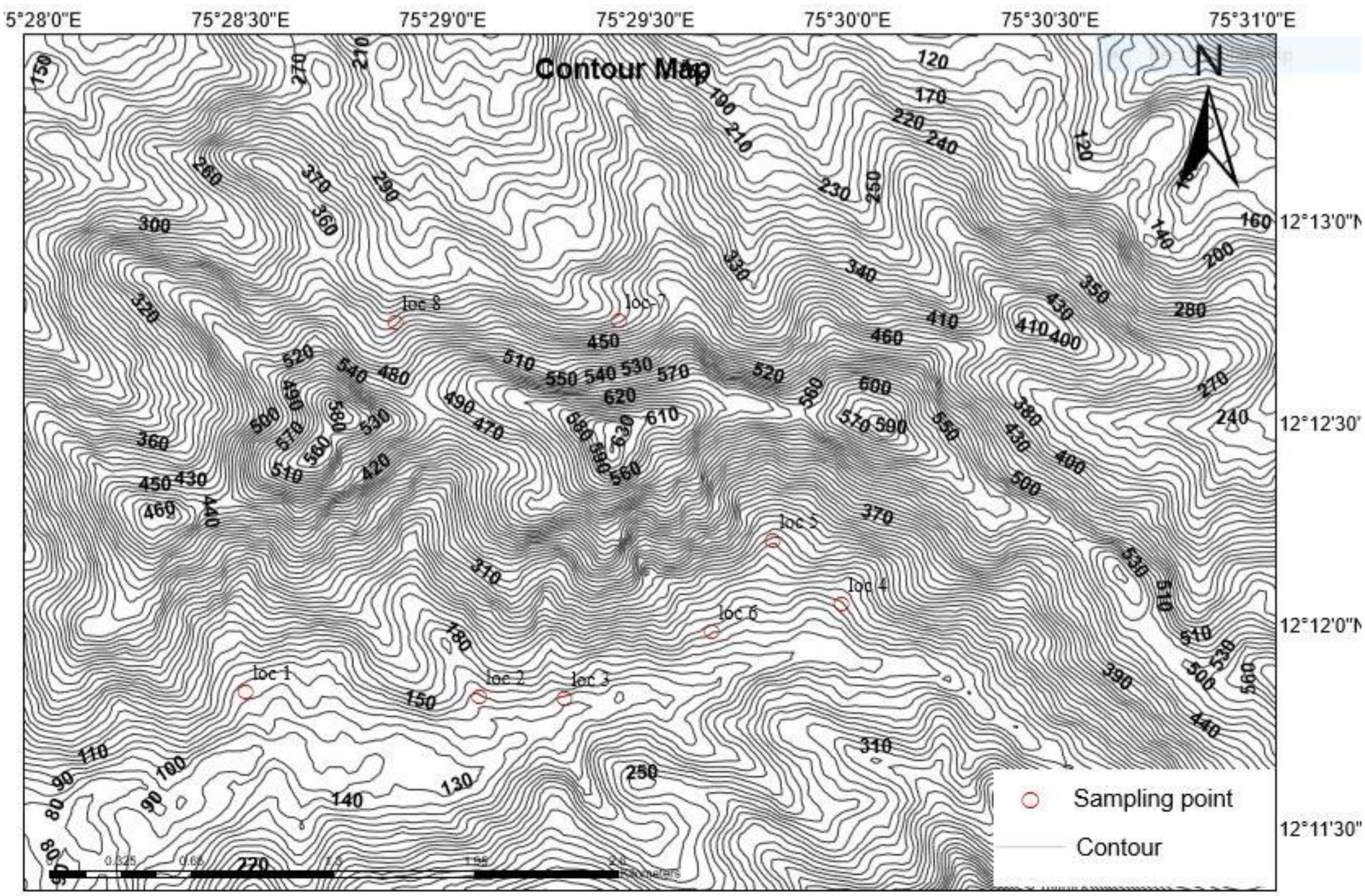

Fig. 3.2 Contour map of the study area in Ottathai

The contour map was used to analyze the gradient and slope of the topography. It was observed that the density of contour lines correlates with the steepness of the terrain: the more closely packed the contours, the higher the slope. Given the significance of slope in understanding the nature of the landscape and correlating it with other datasets like forest cover, a detailed study on the slope of the study area was required. Western Ghats receives high annual precipitation. This elevated precipitation contributes significantly to the water supply and is a prominent weathering agent that shapes the landscape. Over time, water and other weathering agents have extensively modified the slope characteristics of these regions. Consequently, it was anticipated that areas experiencing more significant precipitation would exhibit steeper slopes due to the erosive effects of water and weathering processes.

The subsequent topographical feature examined in this study was the slope. It was necessary to acquire slope data from digital elevation models (DEMs) to investigate the correlation between chemical weathering and slope. These DEMs provided information about the gradient of the terrain, facilitating an analysis of the relationship between slope and chemical weathering processes. Moreover, the extracted slope data were utilized for further analysis, particularly in correlation with tree cover. The slope of the Tamhini study area (Fig. 3.3) is slightly higher than that of the Ottathai study area (Fig. 3.4). The highest slope in the Tamhini region goes up to 80 °, and in the Ottathai study area, the highest slope value is around 70°.

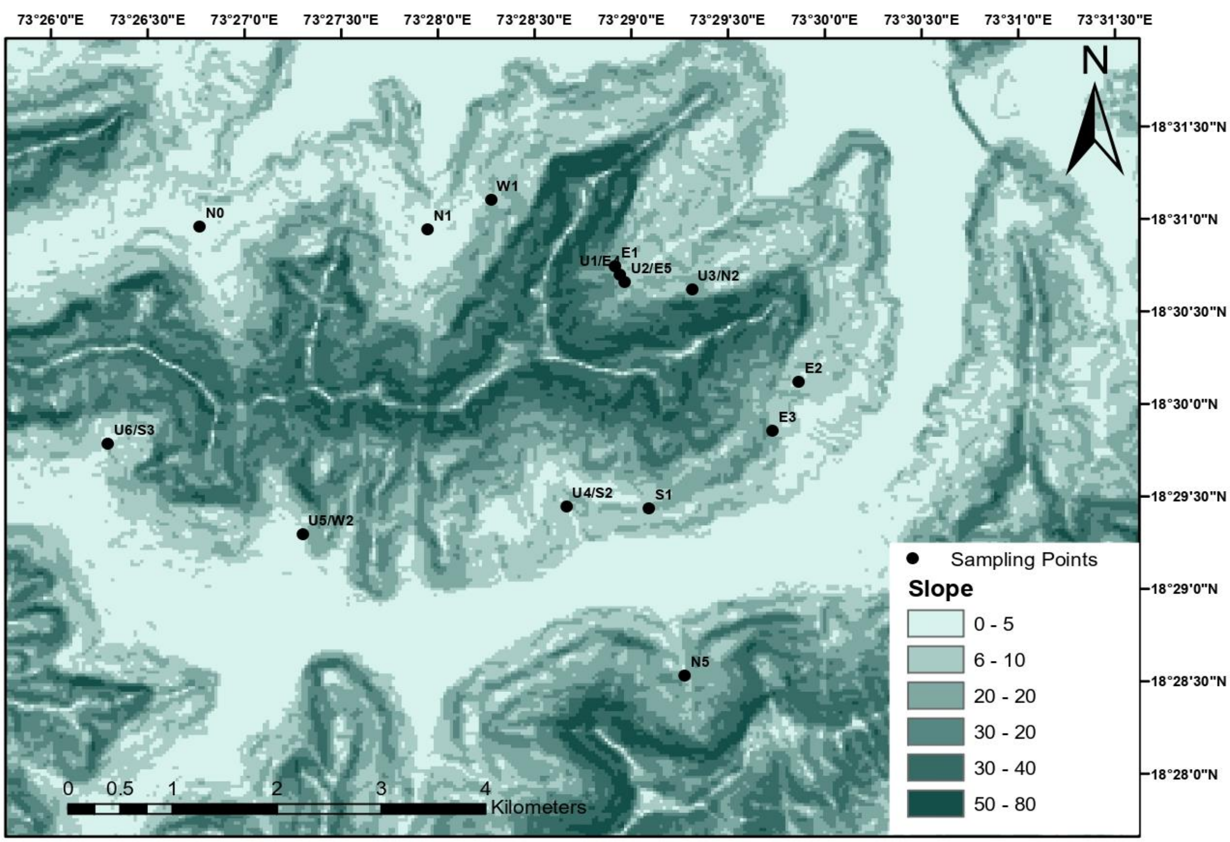

Fig. 3.3 Map showing the slope of the Tamhini study area with sampling points

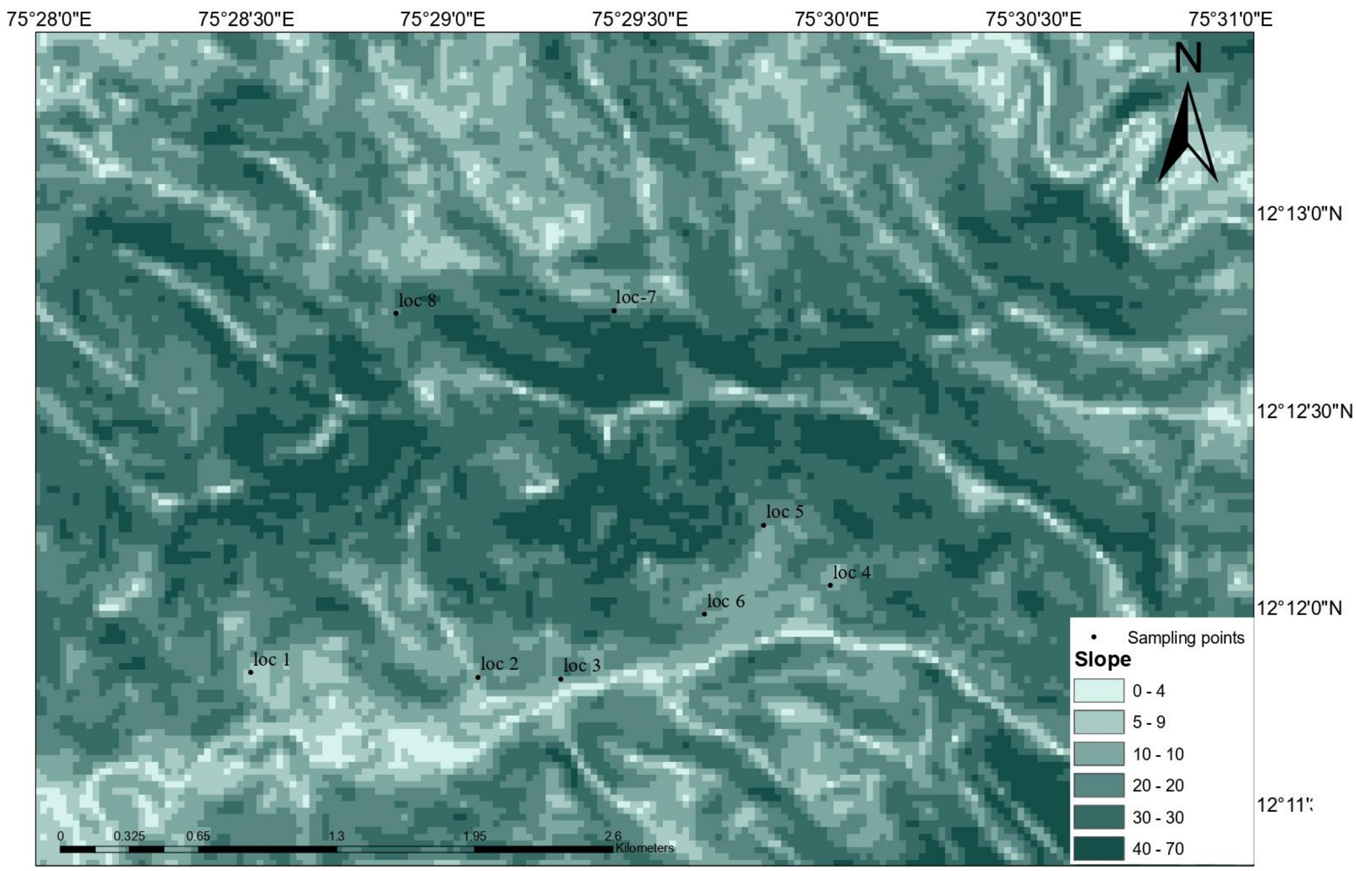

Fig. 3.4 Map showing the slope of the Ottathai study area with sampling points

The maps give us a general idea of how the slopes vary among different sides of the hill section. Utilizing Geographic Information Systems (GIS) software, water channel drainage patterns were delineated, and watershed boundaries were established based on slope and altitude profiles. Topographic maps obtained from the Survey of India datasets were used to validate the accuracy of the GIS-derived drainage pattern. The water channels from the Tamhini ghat (Fig. 3.5) study area contribute to Mulshi Lake, which serves as a crucial reservoir for water supply and hydroelectric power generation. The water channels of the study area in Kerala (Fig. 3.6), the water channels within the study area contribute to the Alakkode River, a major tributary of the Kuppam River. The Kuppam River traverses Kerala from east to west before merging into the Arabian Sea.

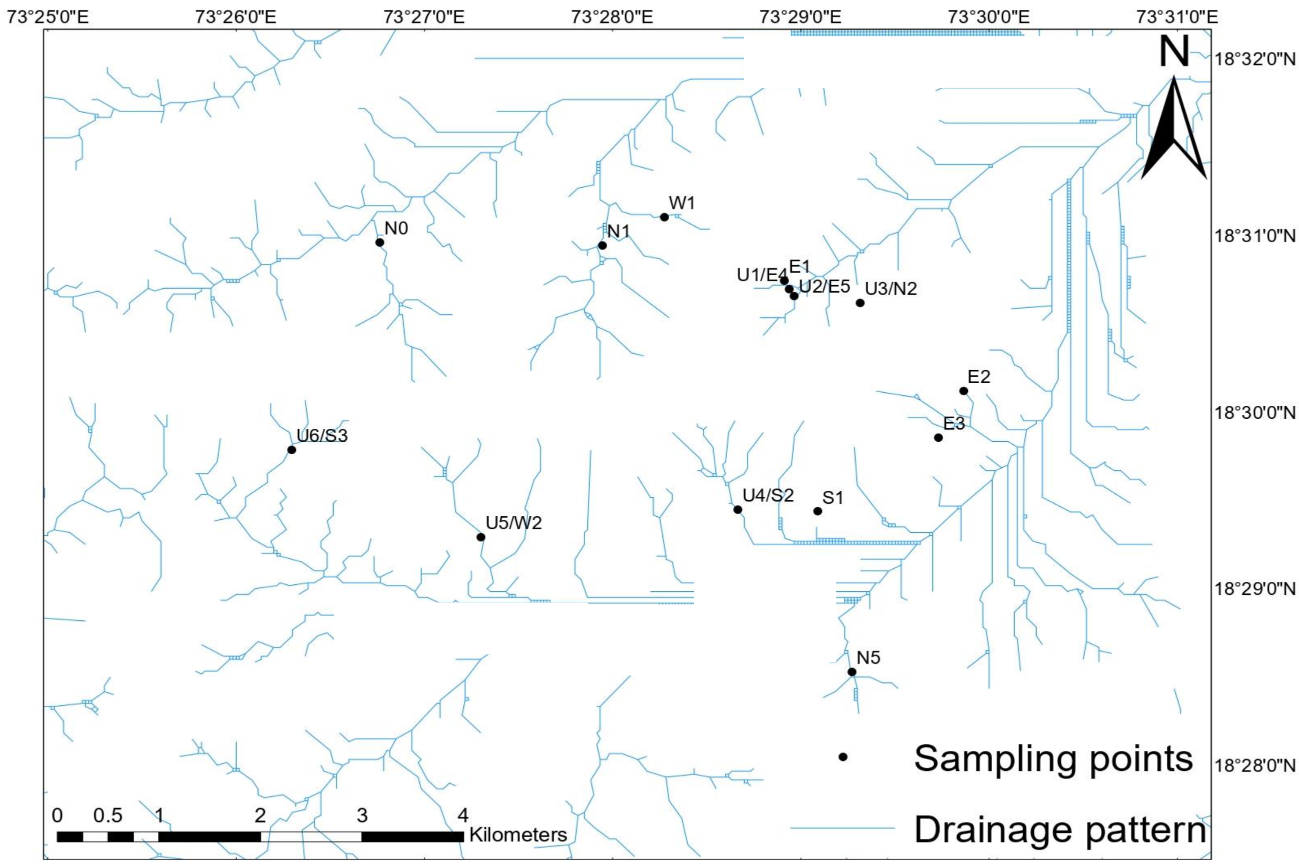

Fig. 3.5 Drainage patterns of the Tamhini study area

The watersheds of the drainage systems were delineated for a detailed study of their respective areas. Small watersheds, clearly defined areas of water flow, were created for the study and have been studied to improve understanding of how local ecosystems function (Likens, 1997). Small streams provide a chance to more precisely understand the factors affecting chemical weathering. We can also learn more by comparing the chemical makeup of various small streams. Small catchments are usually found near the beginning of a river basin, often in mountainous areas. They represent a specific weathering environment more accurately than larger watersheds (Oliva et al., 2003). As the watersheds being examined are small and located in forested areas with minimal human influence, we can ignore the impact of anthropogenic input on ion concentration in this study.

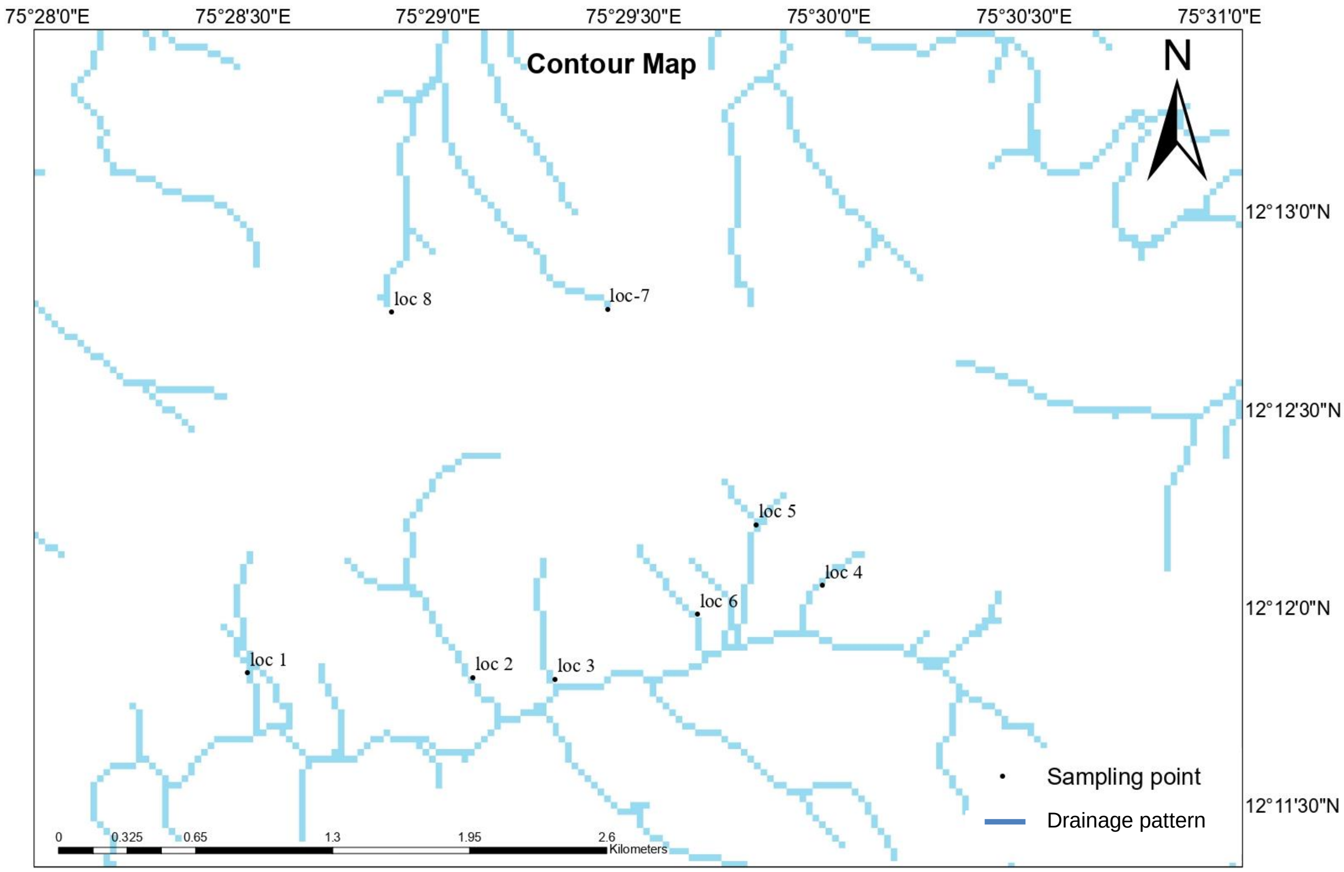

Fig. 3.6 Drainage patterns of the Ottathai study area

The study areas of Tamhini and Ottathai were examined to understand the sizes and shapes of the watersheds present. Specifically, in the Tamhini region, which has 14 watersheds, it was found that the 'N1' watershed stood out as the largest among them. On the other hand, the watersheds labeled as 'U3/N2' and 'E1' were observed to have the smallest measurements in terms of area.

At the same time, in the Ottathai study region, there are 8 different watersheds. Out of that, ‘Loc-2’ was identified as the biggest in terms of area. The ‘Loc-8’ named watershed has the smallest area. The watershed map and area details are given (Fig. 3.7 & 3.8).

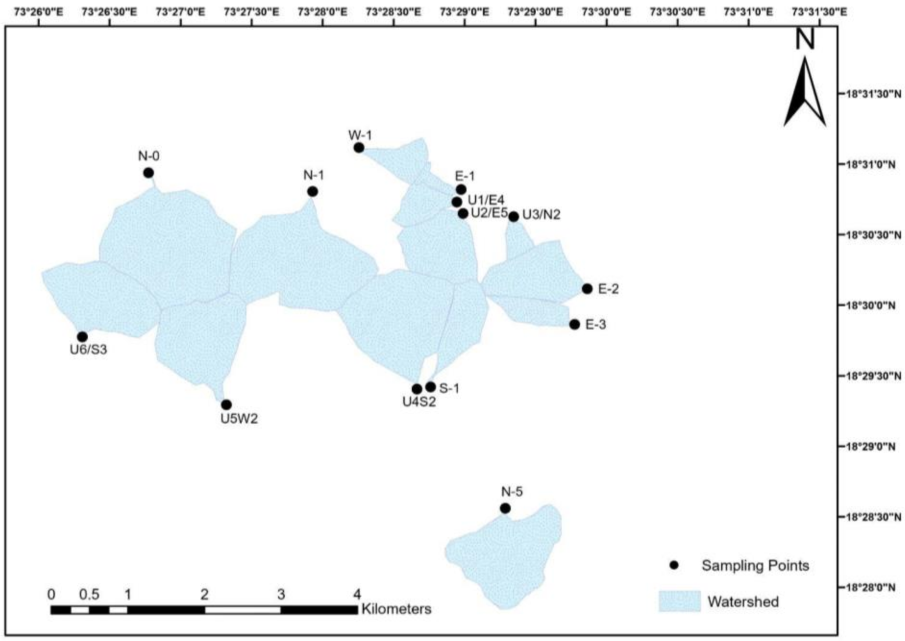

Fig. 3.7 Watershed map of Tamhini study area

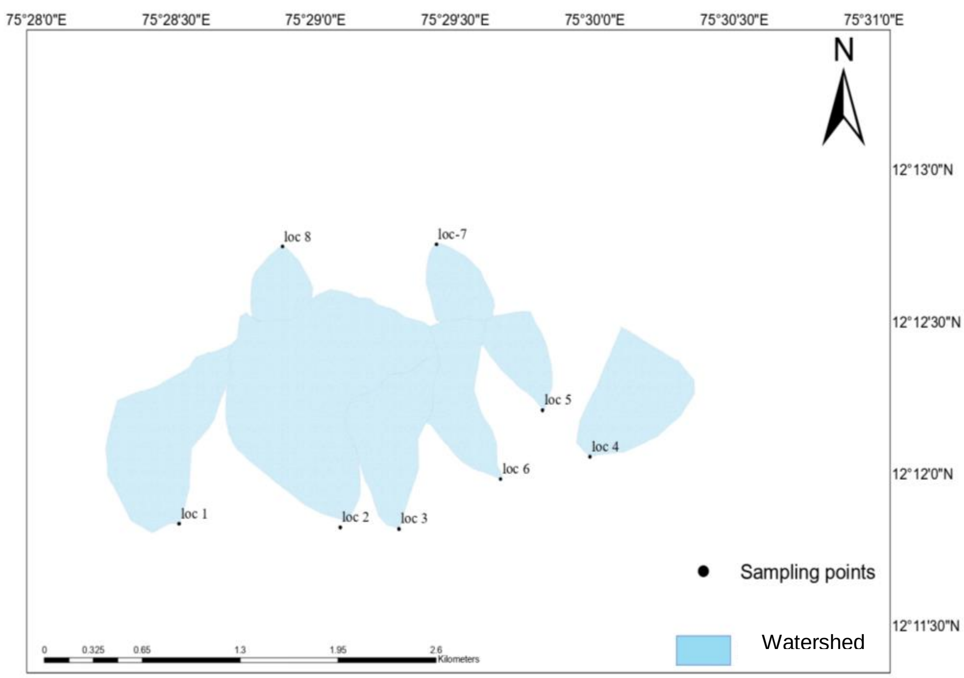

Fig. 3.8 Watershed map of Ottathai study area

NAME	AREA(km^2)
E-1	0.1
E-2	0.63
E-3	0.23
N-0	1.90
N-1	2.47
N-5	1.34
S-1	0.45
U1/E4	0.26
U2/E5	0.68
U3/N2	0.1
U4/S2	1.37
U5/W2	1.00
U6/S3	1.22
W-1	0.25

3.1 Area of Tamhini watersheds

NAME	AREA(km^2)
Loc-1	0.52
Loc-2	1.10
Loc-3	0.36
Loc-4	0.37
Loc-5	0.17
Loc-6	0.28
Loc-7	0.15
Loc-8	0.14

3.2 Area of Ottathai watersheds

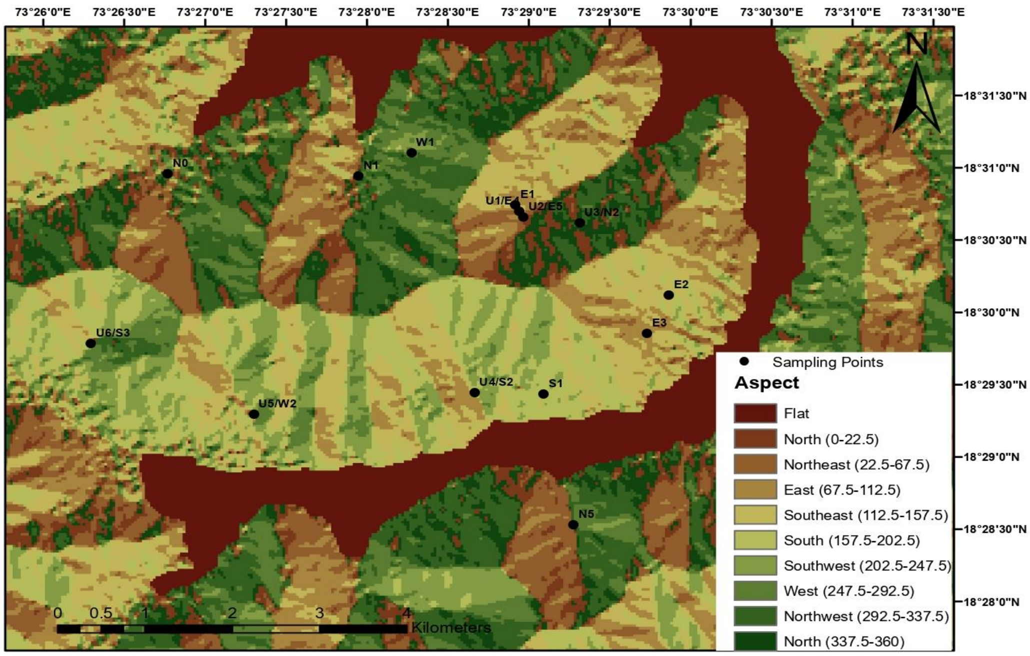

Fig. 3.9 Aspect map of Tamhini study region

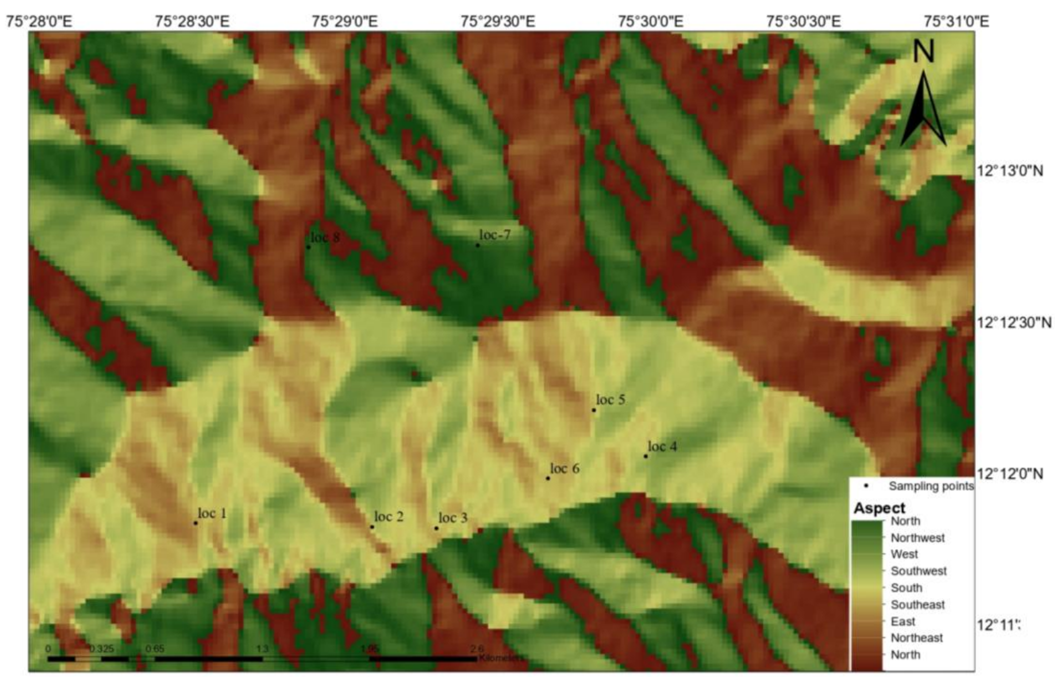

Fig. 3.10 Aspect map of the Ottathai study region

The aspect map of the study area was created to analyze the directional orientation of watersheds. Each watershed was color-coded to represent its aspect, indicating the direction it faces. The map provides valuable insights into the spatial distribution of slope orientations within the study area. Watersheds exhibit diverse aspect orientations, reflecting the topographic complexity of the study area. The aspect maps of Tamhini (Fig. 3.9) and Ottathai (Fig. 3.10) are given.

The slope, aspect, altitude, tree cover, and NDVI values have been opened in Excel and organized such that each pixel value is accompanied by its corresponding parameter values. The mean slope and forest cover data for individual watersheds were calculated for correlation with ion concentrations.

3.2 Analysis of Ion Concentrations

Name	Ca (μM)	Mg (μM)	Na (μM)	pH	Tempertaure (°C)
W1	236	136	158	7.52	25.2
U6S3	163	102	127	7.12	25.7
U5W2	199	127	139	6.75	26.6
U4S2	163	92	128	6.85	25
U3N2	200	95	150	6.02	23.5
U2E5	209	135	156	6.62	23.6
U1E4	211	122	157	6.3	24
S1	190	112	155	7.6	26.4
N5	143	73	126	7.87	25.8
N1	176	104	132	7.56	25
E3	278	190	183	6	24.6
E2	251	138	171	6.99	25.1
E1	200	104	150	6.88	24.5

Table. 3.3 Major ion concentrations and on-field measured pH and temperature values of the Tamhini study area during the 2022 monsoon season.

The cation and anion concentrations of the samples taken from Tamhini and Ottathai were studied. Samples were collected from Tamhini during two monsoon seasons (2022 and 2023) to analyze the temporal characteristics of ion concentrations. Additionally, samples from three months of the 2023 monsoon season were collected from Tamhini to obtain more detailed information about a single monsoon season. The Ottathai (Kerala) samples were collected to examine the trend of ion concentration in the southern region of the Western Ghats compared to the northern region and assess whether the same parameters influence the weathering processes.

Name	Ca (μM)	Mg (μM)	Na (μM)
W1	155	103	133
U6S3	79	99	122
U5W2	109	105	137
U4S2	113	103	141
U3N2	92	109	132
U2E5	117	136	155
U1E4	115	134	155
S1	121	103	135
N5	92	94	126
N1	114	106	139
E3	213	178	184
E2	185	166	190
E1	167	154	182
N0	93	87	126

Table. 3.4 Major ion concentrations and on-field measured pH and temperature values of the Tamhini study area during 2023 July.

Name	Ca (μM)	Mg (μM)	Na (μM)	pH	Tempertaure (°C)
W1	154	155	153	7.26	23.2
U6S3	143	65	106	7.03	23.3
U5W2	153	85	110	6.99	23.9
U4S2	138	81	130	7.07	22.7
U3N2	127	77	121	6.07	22.6
U2E5	149	137	135	7.05	22.7
U1E4	165	143	133	7.1	22.8
S1	146	100	143	7.67	24.5
N5	127	72	97	5.98	22.7
N1	139	86	118	6.19	22.6
E3	209	175	188	6.24	24.6
E2	238	190	186	7.19	23.6
E1	238	159	140	7.03	22.8
N0	109	76	126	5.61	23.2

Table. 3.5 Major ion concentrations and on-field measured pH and temperature values of the Tamhini study area during 2023 August.

The concentration of major cations and anions in the study areas has been examined. In each study area, nitrates exhibit deficient concentrations. In the 2022 monsoon sample, its concentration is lower than the instrument's detection limit. It is observed that there is no specific pattern of ion concentration over the months of the same monsoon season. Depending on the rate of rainfall, it can vary. The significant pattern obtained from the given data is that the concentration of cations is highest in the eastward-facing watersheds. The lowest ionic concentration is found in the watersheds facing north. The order of concentration is decreasing from east, west, south, and north, respectively. The forest cover data extracted from the satellite data sets was also studied, and the watershed facing the north side had the highest tree cover. Followed by south, west, and east at the end. The study of watershed slopes shows a clear pattern: the eastern slopes are steepest, followed by the west, south, and north. Interestingly, this pattern matches the trend in ionic concentration we observed.

Name	Ca (µM)	Mg (µM)	Na (µM)	pH	Tempertaure (°C)
W1	155	140	160	7.16	24
U6S3	137	130	134	7.06	29
U5W2	158	135	146	6.77	26.8
U4S2	137	124	129	6.72	25.2
U1E4	165	143	150	6.43	23.7
S1	142	130	160	6.21	25.8
N5	104	123	127	7.46	22.3
N1	130	130	134	7.23	23.8
E1	166	145	152	6.77	23.9
N0	108	128	128	6.35	24.1

Table. 3.6 Major ion concentrations and on-field measured pH and temperature values of the Tamhini study area during 2023 September.

Name	Ca (µM)	Mg (µM)	Na (µM)	pH	Tempertaure (°C)
loc 1 (W2)	85	110	117	7.31	26.2
loc 2 (N1)	58	66	110	7.34	25.9
loc 3 (S1)	87	122	141	7.71	26
loc 4 (S2)	70	92	131	7.34	25.7
loc 5 (S3)	55	90	125	7.04	25.9
loc 6 (E1)	52	71	86	7.6	26.1
loc 7 (E2)	48	69	102	5.95	26.1
loc 8 (W1)	53	84	125	6.89	25.6

Table. 3.7 Major ion concentrations and on-field measured pH and temperature values of the Ottathai study area during the 2023 late monsoon

The relationship between ionic concentration, slope, and tree cover presents a unique scenario. Usually, we anticipate higher ion concentrations in areas with higher tree cover. However, our observations contradict this expectation. In this case, watersheds with steeper slopes and the lowest tree cover (east) have the highest ionic concentration, indicating that the higher the slope, the higher the chemical weathering. Regarding tree cover, the higher the tree cover, the lesser the chemical weathering. From east to north, this trend is visible for samples collected from Tamhini and Ottathai. Accuracy and precision were also measured by analyzing cation and anion concentrations. The error percentages for anions are 3% for Cl, 2.1% for SO4, and 5% for NO3. Repeated analysis of samples using ion chromatography was conducted to assess the precision of the data. A 0% difference was observed between two runs of the same sample, concluding that the data is precise. For cation analysis, the error percentages are 1% for Na, 0.2% for Ca, and 3% for Mg. A 3% difference was observed upon repeated analysis of the data. The cation data is also considered precise and accurate based on the calculations.

3.3 Analysis of Silica Concentrations

The silica concentration of samples was measured using spectrophotometer (Table. 3.2).

Name	Conc. (μM)
w1	133
u6s3	122
u5w2	137
u4s2	141
u3n2	132
u2e5	155
u1e4	155
s1	135

Name	Conc. (μM)
w1	153
u6s3	106
u5w2	110
u4s2	130
u3n2	121
u2e5	135
u1e4	133
s1	143

n5	126
n1	139
e3	184
e2	190
e1	182
n0	126

Table. 3.8 Silica concentration of 2023 July Tamhini samples

n5	97
n1	118
e3	188
e2	186
e1	140
n0	126

Table. 3.9 Silica concentration of 2023 August Tamhini samples

Name	Conc. (μM)
w1	160
u6s3	134.4
u5w2	146.3
u4s2	128.5
u1e4	150.2
s1	160
n5	126.6
n1	134.4
e1	152.2
n0	128

Table. 3.10 Silica concentration of 2023 September Tamhini samples

Name	Conc. (μM)
e1(l6)	138.8487
s3(l5)	113.8996
e2(l7)	147.5426
w1(l8)	116.9763
w2(l1)	102.8327
n(l2)	76.71509
s1(l3)	81.40302
s2(l4)	105.0461

Table. 3.11 Silica concentration of Ottathai samples from 2023 December

The silica concentration in the water samples can give insights into the silicate weathering of rocks. The pattern of the relationship between tree cover and cation concentration is also visible in the silicate concentration. The watersheds with higher tree cover have lesser silica concentration. The relationship with the slope is also the same, where a high watershed facing the east has a higher slope and a higher silica concentration. Atmospheric correction is not done for the concentration values.The detailed correlation study was done by plotting the tree cover and slope with cation concentration. All watersheds' average slope and tree cover data are given in Table. 3.2(e).

Name	Average tree cover (%)	Average slope
w1	15.1	26.2
u6s3	31.1	23.7
u5w2	18.4	25.0
u4s2	31.1	24.0
u3n2	32.5	21.5
u2e5	13.6	27.1
u1e4	9.9	29.9
s1	22.9	23.9
n5	37.3	21.6
n1	31.9	21.9
e3	0.2	29.6
e2	0.5	26.9
e1	9.0	29.0
n0	25.2	19.4
e1(l6)	15.0	27.3

s3(l5)	41.9	23.8
e2(l7)	13.7	29.5
w1(l8)	29.5	24.3
w2(l1)	30.8	25.7
n(l2)	50.0	20.5
s1(l3)	45.5	23.3
s2(l4)	44.1	21.1

Table. 3.12 Average tree cover and forest cover of all watersheds combined

3.4 Correlation analysis

The cation concentration and the silicate concentration act as the indicators of chemical weathering. By correlating them with the tree cover and slope, we aim to figure out the factors controlling chemical weathering in the study area. A positive correlation was expected between tree cover and ion concentration data, as tree cover enhances weathering using organic acids. The second scenario is tree cover limiting the chemical weathering. An interpretation can be made by analyzing the correlation data on the factors influencing chemical weathering.

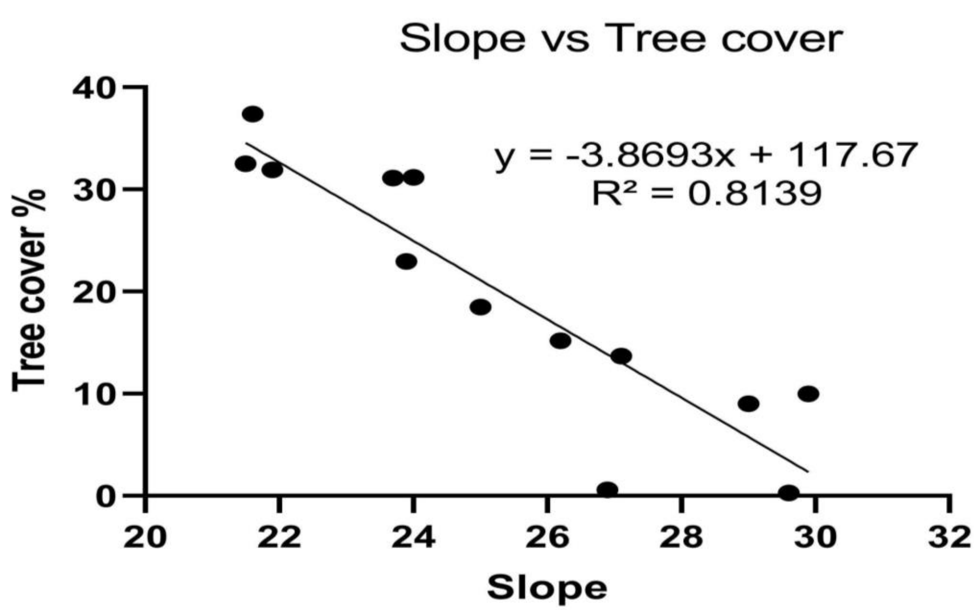

Fig. 3.11 Tree cover vs Slope plot of Tamhini (p value = 0.00001)

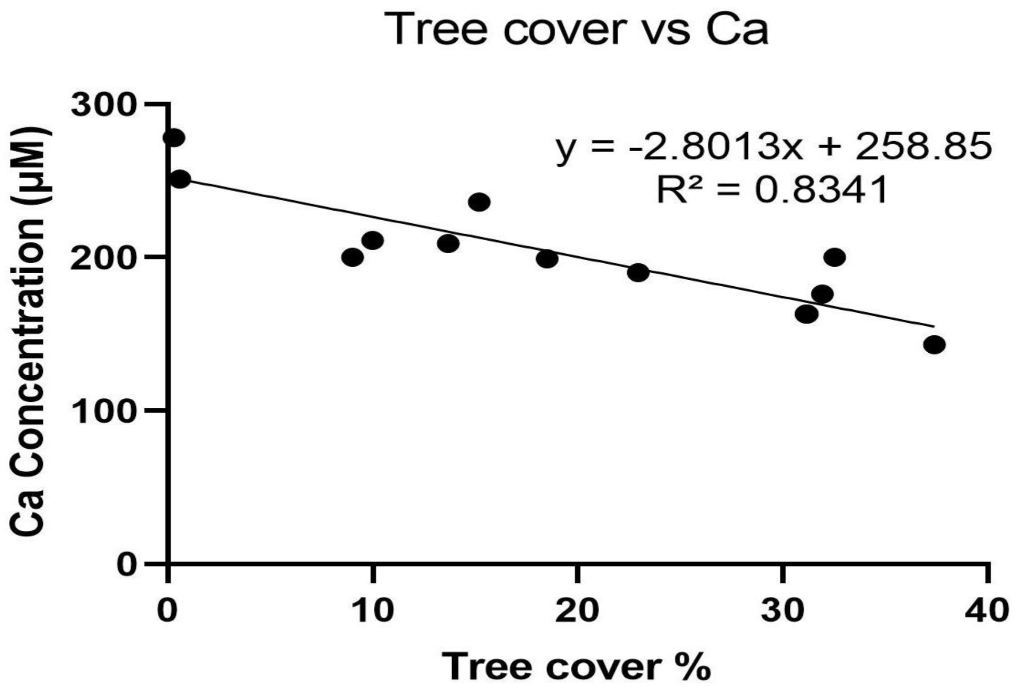

Fig. 3.12 Tree cover vs Ca (2022 Monsoon season) (p value = 0.000013)

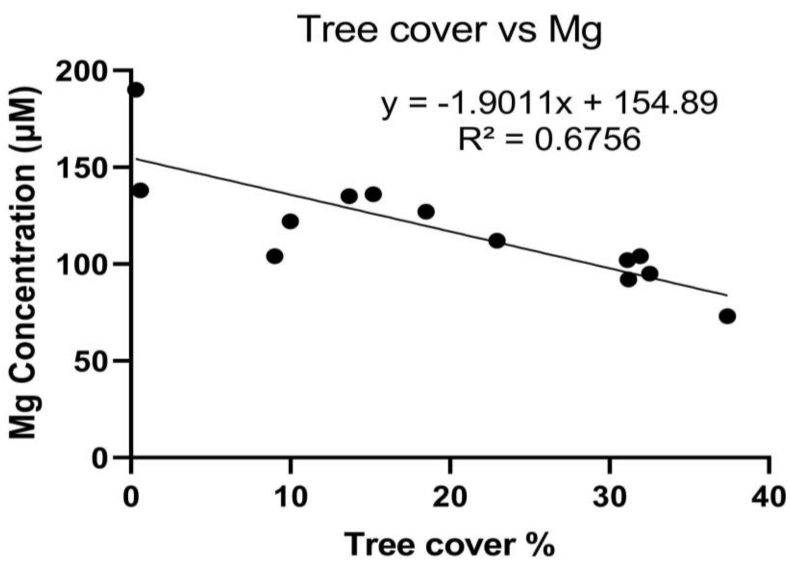

Fig. 3.13 Tree cover vs Mg (2022 Monsoon season) (p value = 0.000581)

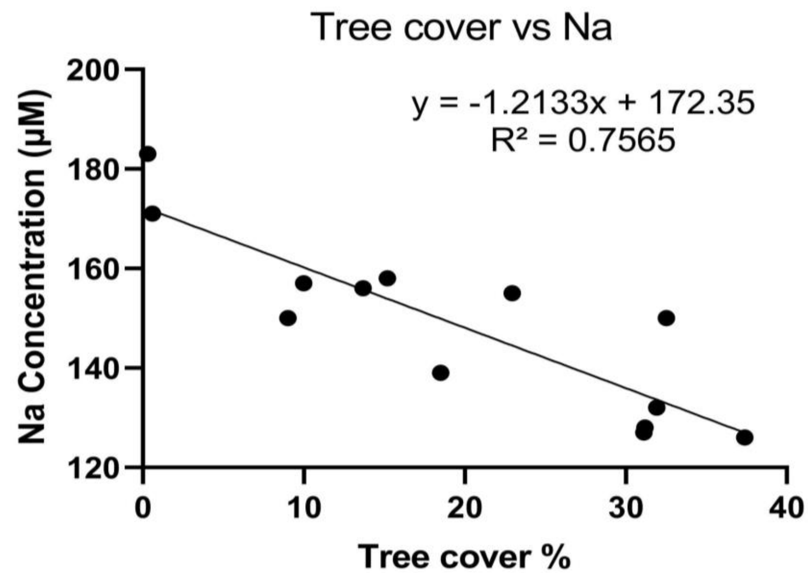

Fig. 3.14 Tree cover vs Na (2022 Monsoon season) (p value = 0.000115)

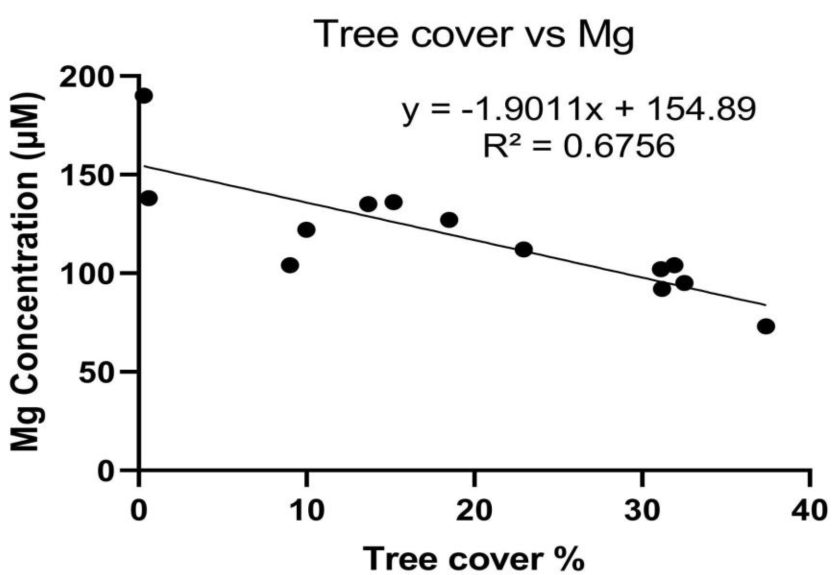

Fig. 3.15 Tree cover vs Mg (2023 July) (p value = 0.000319)

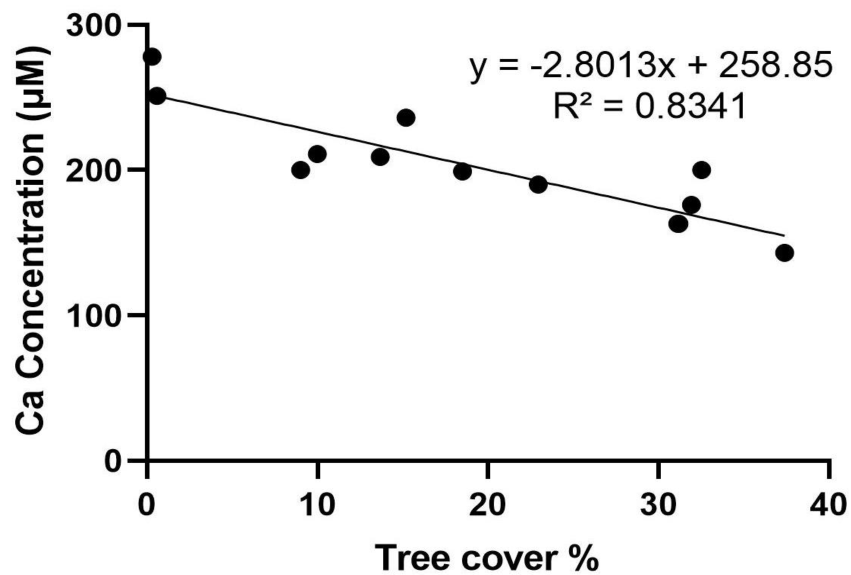

Fig. 3.16 Tree cover vs Ca(2023 July)(p value = 0.00001)

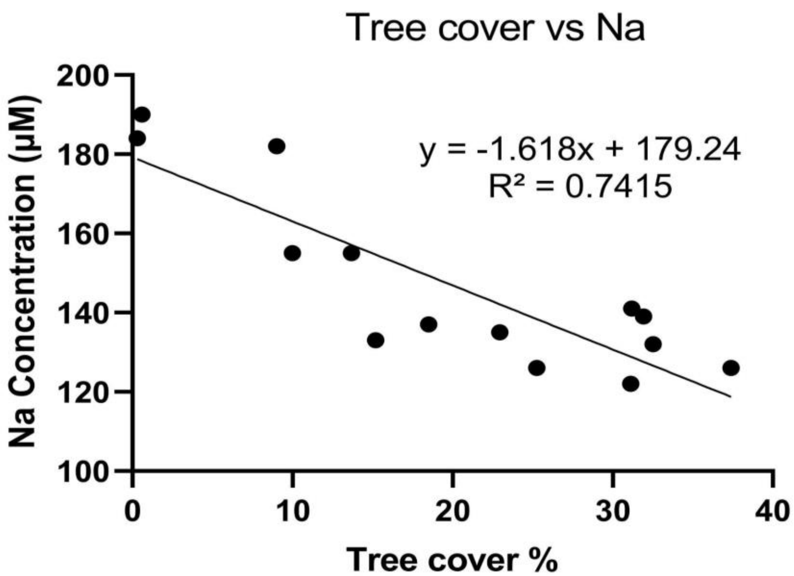

Fig. 3.17 Tree cover vs Na (2023 July) (p value= 0.000077)

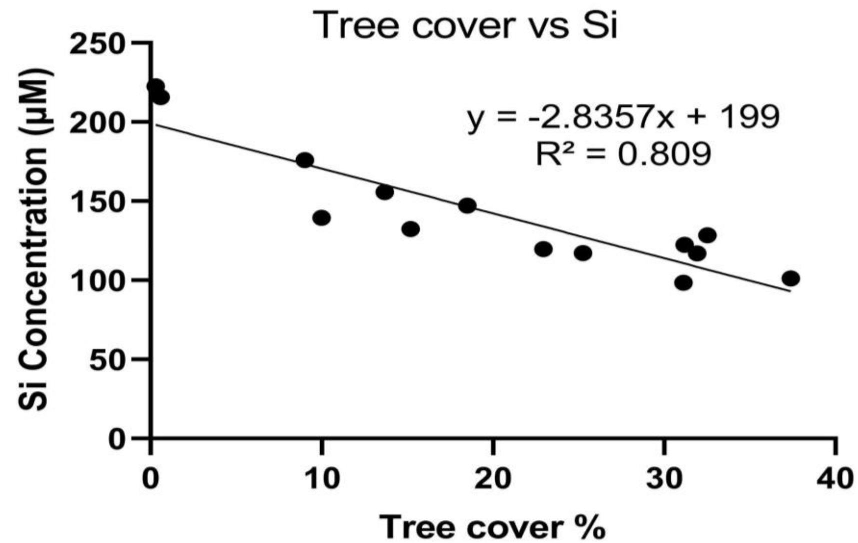

Fig. 3.18 Tree cover vs Si (2023 July) (p value = 0.000012)

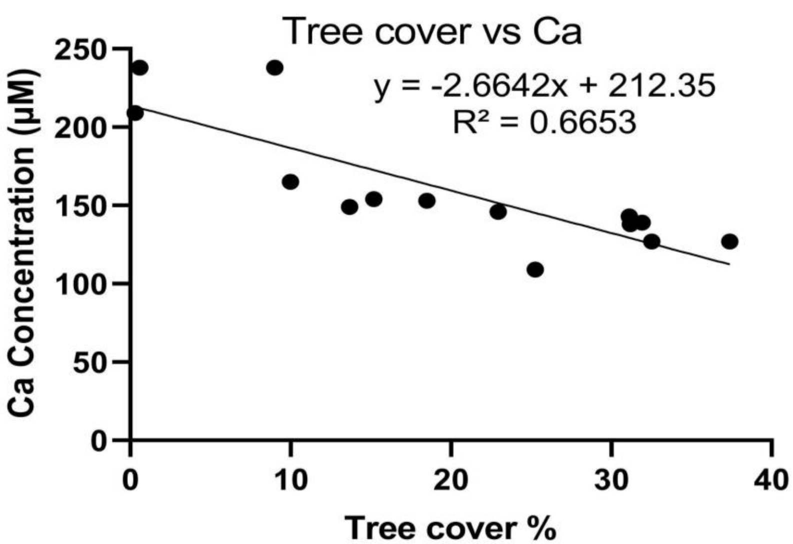

Fig. 3.19 Tree cover vs Ca(2023 August) (p value = 0.000377)

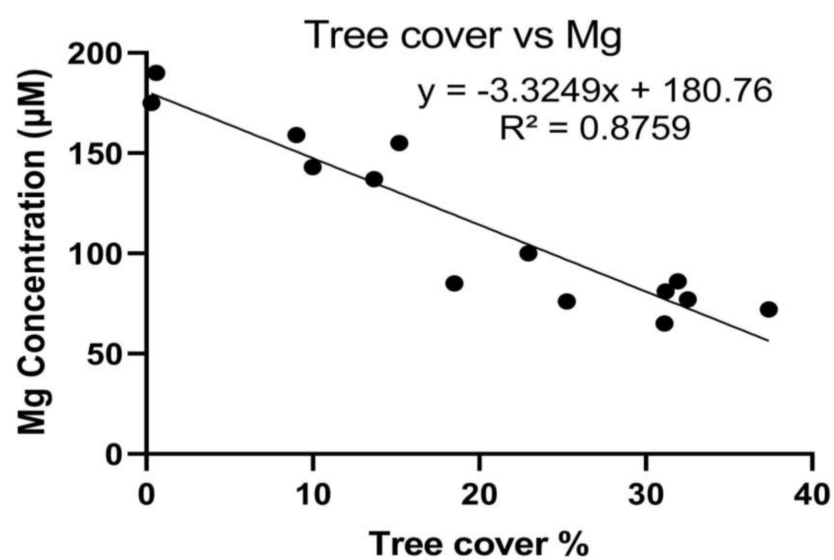

Fig. 3.20 Tree cover vs Mg (2023 August) (p value = 0.00001)

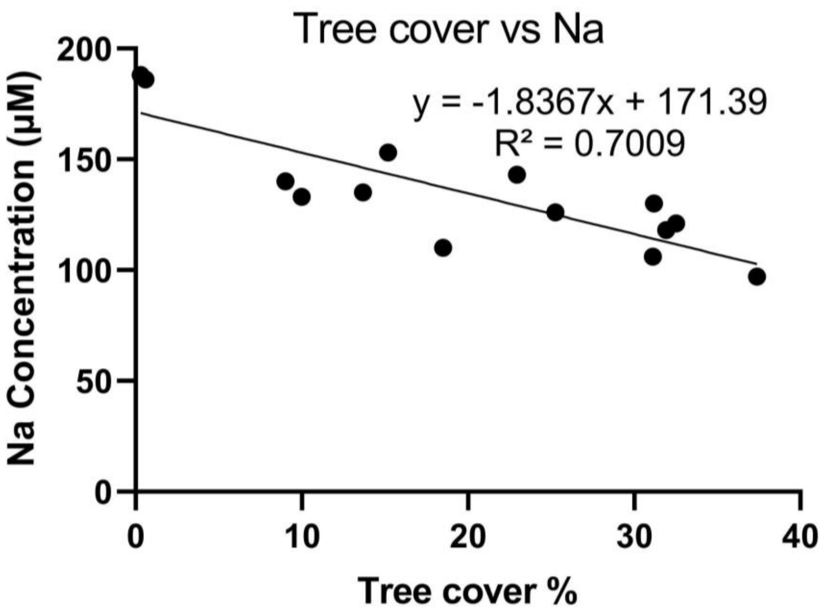

Fig. 3.21 Tree cover vs Na (2023 August) (p value = 0.000188)

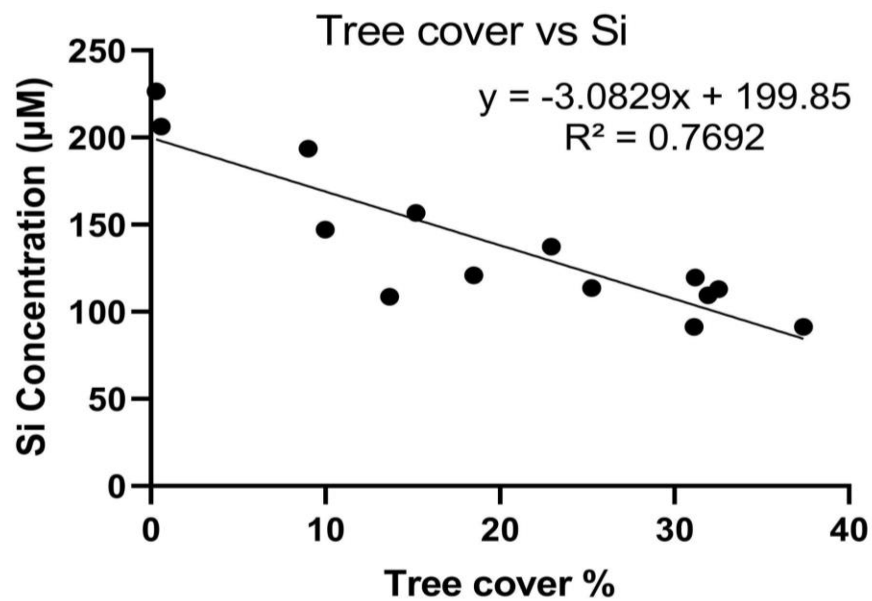

Fig. 3.22 Tree cover vs Si (2023 August) (p value = 0.000038)

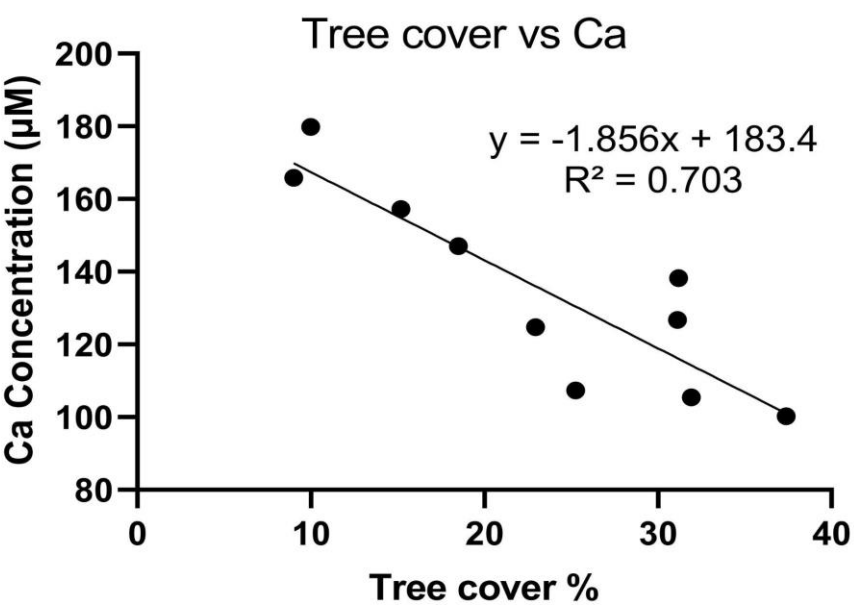

Fig. 3.23 Tree cover vs Ca (2023 September) (p value = 0.000182)

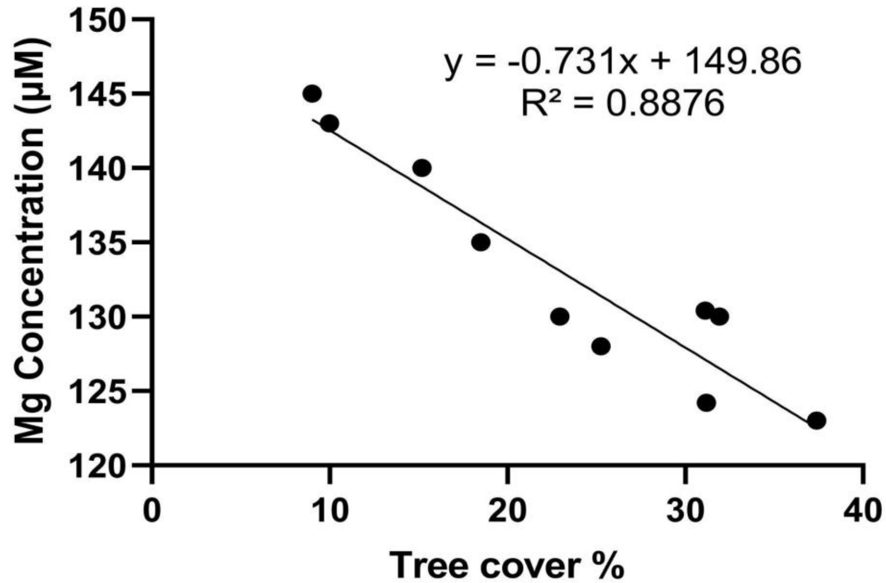

Fig. 3.24 Tree cover vs Mg (2023 September) (p value = 0.00001)

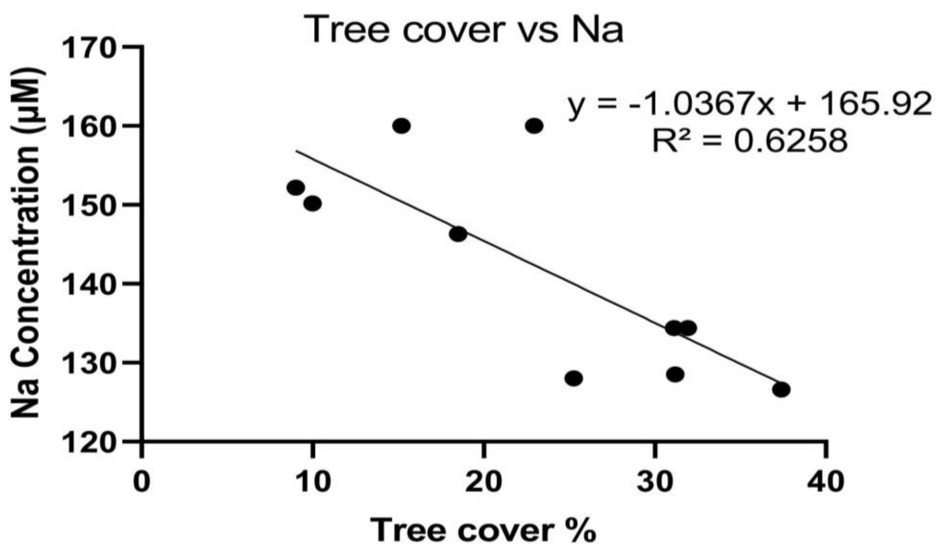

Fig. 3.25 Tree cover vs Na (2023 September) (p value = 0.000754)

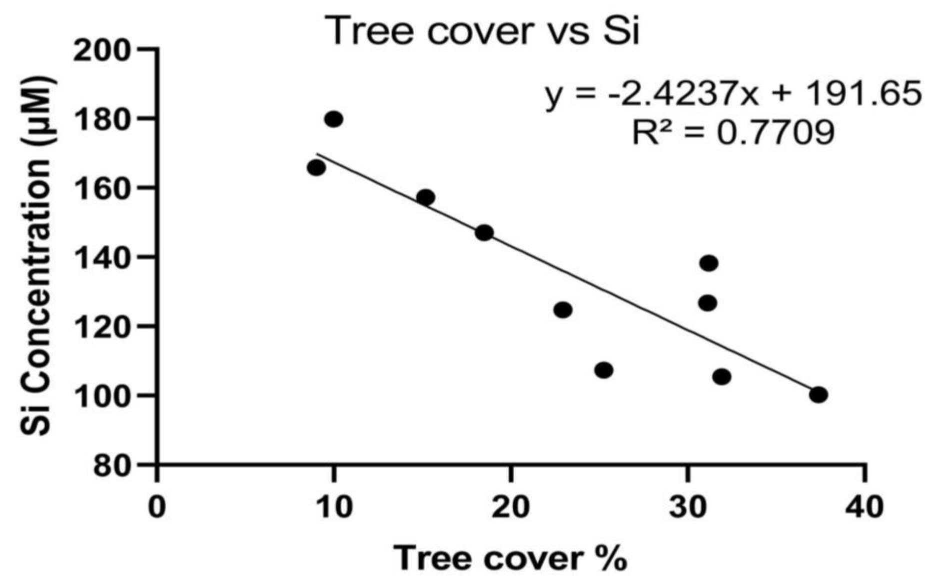

Fig. 3.26 Tree cover vs Si (2023 September) (p value =0.000036)

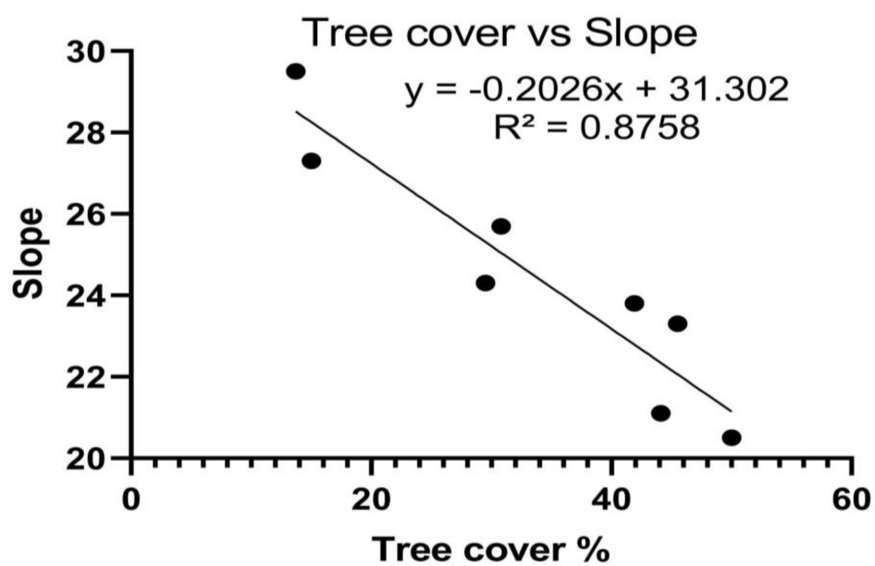

Fig. 3.27 Tree cover vs Slope plot of Ottathai study area (p value = 0.00063)

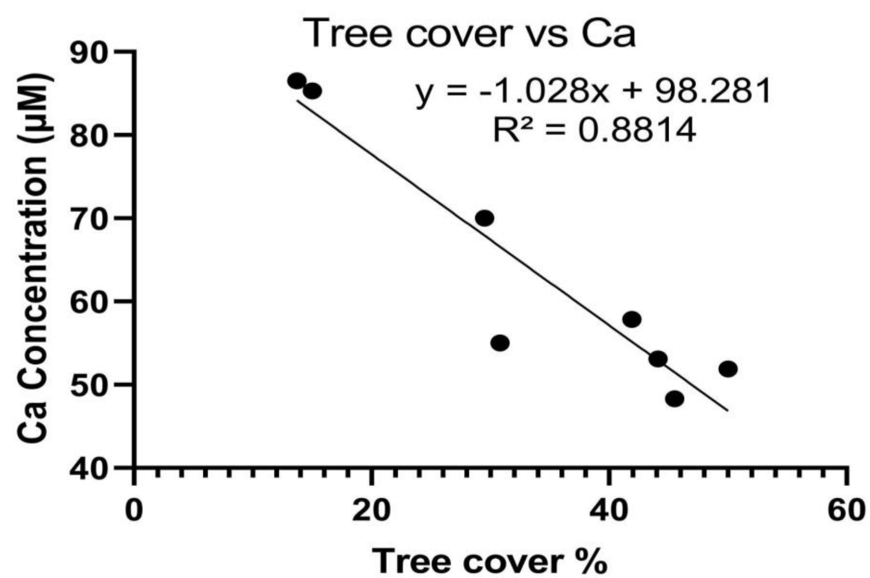

Fig. 3.28 Tree cover vs Ca (2023 December) (p value = 0.000547)

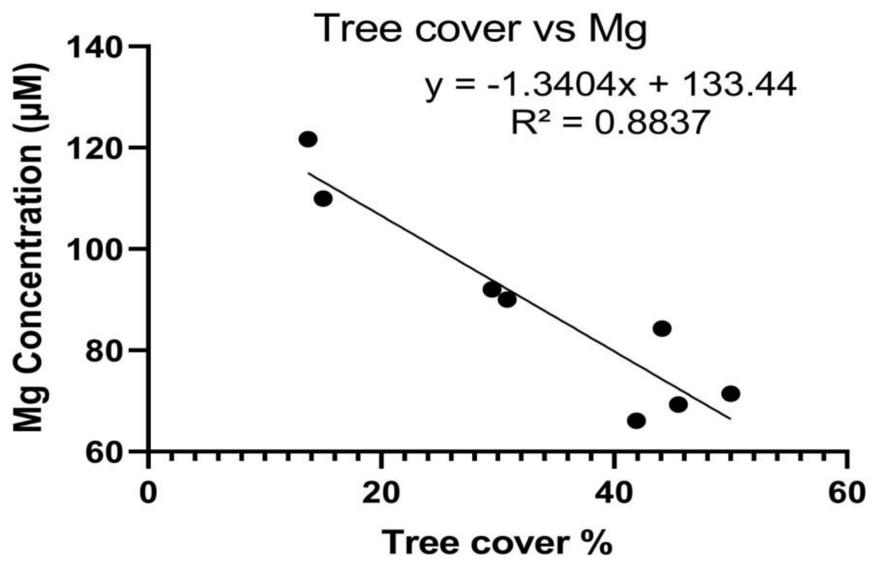

Fig. 3.29 Tree cover vs Mg (2023 December) (p value = 0.000516)

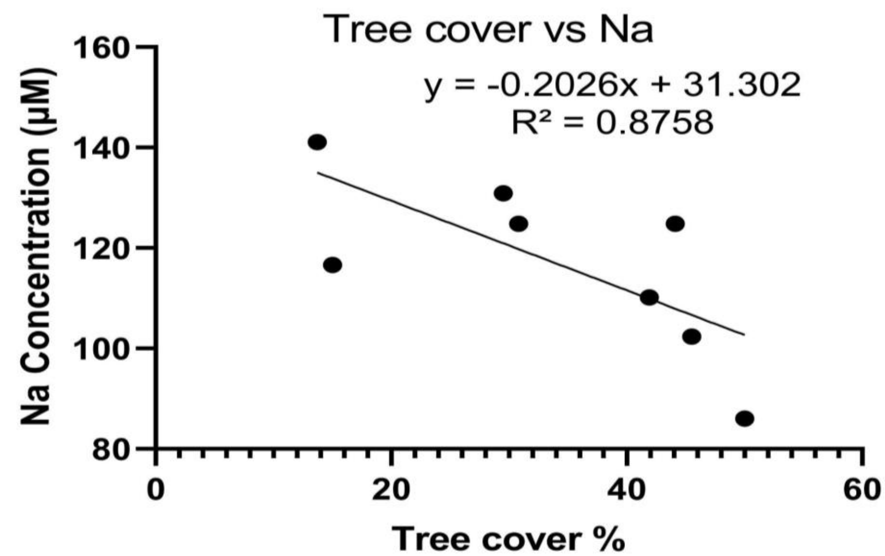

Fig. 3.30 Tree cover vs Na (2023 December) (p value = 0.00063)

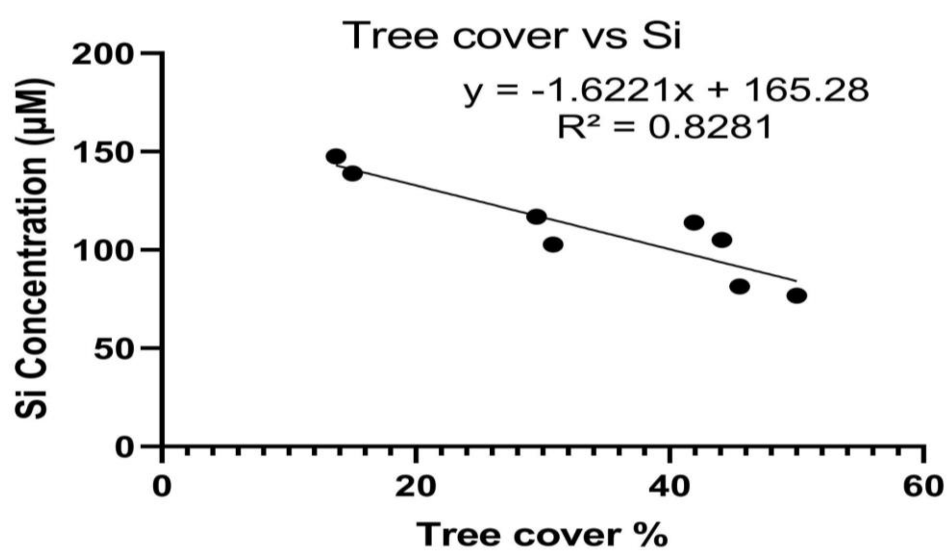

Fig. 3.31 Tree cover vs Si (2023 December) (p value = 0.00170)

The correlation analysis between tree cover, slope, and cation concentrations reveals clear patterns. Firstly, there is a negative correlation between slope and tree cover, as well as between tree cover and ion concentration. Figures 3.11 to 3.26 illustrate the analysis for the Tamhini samples, while Figures 3.26 to 3.31 depict the results for the Ottathai samples. The 2022 samples show a strong negative correlation (r2 = 0.81) between tree cover and calcium (Ca) concentration. Similarly, sodium (Na) and magnesium (Mg) also exhibit negative correlations, indicating that higher tree cover corresponds to lower cation concentration. This trend persists in the July, August, and September 2023 samples. Although Na concentration shows a slightly smaller r^2 value, the negative correlation remains consistent across samples, including those from Ottathai. Samples from the same monsoon season (2023) consistently display this correlation, suggesting no variation within or across seasons. Notably, Ottathai samples from Kerala exhibit a similar trend, indicating consistency in the southern part of the Western Ghats. Cation concentrations in Ottathai are slightly lower than in Tamhini, possibly due to greater tree cover.

Based on the observations above, tree cover does not facilitate chemical weathering in the study areas; instead, it inhibits it. This inhibition could be attributed to the presence of soil cover on top of the parent rock. The tree cover helps retain soil, creating a protective layer over the parent rock, thus inhibiting its weathering process. The percolating rainwater likely travels mostly through the soil and do not come in contact with the fresh rock. The concept of supply-limited and kinetic-limited weathering is studied here.

3.4.1 Transport limited & Kinetic limited weathering

In kinetically limited weathering, the speed of mineral dissolution or reaction with water and other substances mainly controls the weathering process. Unlike factors like how much water is available or the rock's surface area, it is the rate of these chemical reactions that matters most. This kind of weathering typically happens in places where the chemical reactions involved in weathering move slowly, like in colder climates or in rocks that are not very reactive.

When there is an ample supply of water and acid relative to the quantity of silicate minerals, and these minerals spend an extended period in the weathering environment, they undergo alterations before being removed. When the removal process operates at a slower pace compared to the rate of chemical weathering, the weathering process is described as "transport-limited." After the change in climate or weathering rate, there should be some amount of time for balancing the chemical weathering rate and material supply, during this time formation of thick soil cover occurs(West et al., 2005). When the soil and weathered particles are accumulated on the parent rock, supply-limited condition is created. The inherent tendency of weathering to reach a limit is a defining characteristic of stable cratons situated in both temperate and tropical climates. The disturbance of the weathered mantle, in the absence of alterations in the base level, can exclusively occur through the extension of soil movement to extremely low topographic gradients, facilitated by the imposition of a freeze-thaw cycle (Mackay, 1993). The Western Ghats have been relatively stable in recent geological timescales, with climates similar to tropical ones; therefore, the supply limited conditions can be applicable. According to the findings of the study, it appears that supply-limited conditions characterize weathering in the study areas of Western Ghats.

Conclusions

The Western Ghats experience higher precipitation during the monsoon season and boast abundant tree cover. Investigating chemical weathering on this type of landscape by analyzing cation concentrations and correlating them with slope and forest cover data has yielded valuable insights into the limiting factors of chemical weathering in the study areas. The correlation analysis between tree cover and slope, tree cover vs cation and tree cover vs Si data yielded significant results ($P<0.001$). Temporal analysis of cation concentrations across different points in the monsoon season has confirmed a negative correlation between cation concentration and tree cover. This trend is consistent across water samples from the southern part of the Western Ghats, indicating uniformity in weathering limiting factors in the north and south of the Ghats. Higher ion concentrations were observed in east-facing watersheds, where tree cover is lower.

Conversely, lower cation concentrations were recorded in north-facing watersheds with abundant tree cover. The abundant tree cover creates a transport-limited weathering environment in which removal of weathered minerals is slow because of the root system present. This causes creation of thick soil cover above the parent rock, which act as a layer preventing parent rock from weathering. This is a supply-limited condition. So in the study area, tree cover creates a supply-limited system which causes the water samples to have low cation concentration. The study found that vegetation cover does not facilitate silicate weathering but rather inhibits it. The development of soil cover on top of the parent rock restricts weathering by preventing direct contact between the parent rock and water.

Research conducted in tropical forests of the Amazon ("Geochemistry of the Amazon: 3. Weathering Chemistry and Limits to Dissolved Inputs," 1987) and stable continents with tropical climates has highlighted the significance of such climates for supply-limited weathering to occur, a characteristic shared by the Western Ghats. Based on the findings of this study, it is concluded that the study areas of Western Ghats discussed in this project also experience supply-limited weathering, similar to tropical forests in the Amazon.

References

Blum, A. E., & Stillings, L. L. (1995). Chapter 7. FELDSPAR DISSOLUTION KINETICS.

Bluth, G. J., & Kump, L. R. (1994). Lithologic and climatologic controls of river chemistry. *Geochimica et Cosmochimica Acta*, *58*(10), 2341-2359.

Chacko, T., Kumar, G. R. R., & Newton, R. C. (1987). Metamorphic P-T Conditions of the Kerala (South India) Khondalite Belt, a Granulite Facies Supracrustal Terrain. *The Journal of Geology*, *95*(3), 343–358. https://doi.org/10.1086/629134

Cidu, R. (2001). *Water-rock interaction: Proceedings of the tenth International symposium on water-rock interaction, WRI-10, Villasimius, Italy, 10-15 July 2001*. A.A. Balkema.

Cooray, P. G. (1969). Charnockites are metamorphic rocks. *American Journal of Science*, *267*(8), 969–982.

Das, S., Kandekar, A. M., & Sangode, S. J. (2022). Lithologic Controls on Geomorphic Evolution of the Central Western Ghats: An Example from the Aghnashini Catchment, Karnataka, India. *Journal of the Geological Society of India*, *98*(4), 451–459. https://doi.org/10.1007/s12594-022-2001-6

Dove, P. M. (1995). Chapter 6. KINETIC AND THERMODYNAMIC CONTROLS ON SILICA REACTIVITY IN WEATHERING ENVIRONMENTS. In A. F. White & S. L. Brantley (Eds.), *Chemical Weathering Rates of Silicate Minerals* (pp. 235–290). De Gruyter. https://doi.org/10.1515/9781501509650-008

Drever, J. I. (1994). The effect of land plants on weathering rates of silicate minerals. *Geochimica et Cosmochimica Acta*, *58*(10), 2325–2332. https://doi.org/10.1016/0016-7037(94)90013-2

Edmond, J. M., Palmer, M. R., Measures, C. I., Grant, B., & Stallard, R. F. (1995). The fluvial geochemistry and denudation rate of the Guayana Shield in Venezuela, Colombia, and

Brazil. *Geochimica et Cosmochimica Acta*, *59*(16), 3301–3325. https://doi.org/10.1016/0016-7037(95)00128-M

Evans, L. J. (1992). Alteration products at the earth’s surface—The clay minerals. In *Developments in Earth Surface Processes* (Vol. 2, pp. 107–125). Elsevier. https://doi.org/10.1016/B978-0-444-89198-3.50010-6

Gaillardet, J., Dupré, B., & Allègre, C. J. (1995). A global geochemical mass budget applied to the Congo basin rivers: Erosion rates and continental crust composition. *Geochimica et Cosmochimica Acta*, *59*(17), 3469–3485. https://doi.org/10.1016/0016-7037(95)00230-W

Geochemistry of the Amazon: 3. Weathering chemistry and limits to dissolved inputs. (1987). *Journal of Geophysical Research: Oceans*, *92*(C8), 8293–8302. https://doi.org/10.1029/JC092iC08p08293

Ghose, N. C. (1976). Composition and origin of Deccan basalts. *Lithos*, *9*(1), 65–73. https://doi.org/10.1016/0024-4937(76)90057-8

Gunnell, Y. (1997). Relief and climate in South Asia: The influence of the western ghats on the current climate pattern of peninsular India. *International Journal of Climatology*, *17*(11), 1169–1182. https://doi.org/10.1002/(SICI)1097-0088(199709)17:11<1169::AID-JOC189>3.0.CO;2-W

Gupta, R. P. (2017). *Remote sensing geology*. Springer.

Hansen, M. C., Potapov, P. V., Moore, R., Hancher, M., Turubanova, S. A., Tyukavina, A., Thau, D., Stehman, S. V., Goetz, S. J., Loveland, T. R., Kommareddy, A., Egorov, A., Chini, L., Justice, C. O., & Townshend, J. R. G. (2013). High-Resolution Global Maps of 21st-Century Forest Cover Change. *Science*, *342*(6160), 850–853. https://doi.org/10.1126/science.1244693

HEYES, A.; MOORE, T. R. (n.d.). THE INFLUENCE OF DISSOLVED ORGANIC CARBON AND ANAEROBIC CONDITIONS ON MINERAL WEATHERING. *Soil Science 154(3):P 226-236, September 1992.*

https://www.smacgigworld.com/blog/double-beam-spectrophotometer.php

Huang, W. H., & Keller, W. D. (1970). Dissolution of rock-forming silicate minerals in organic acids: Simulated first-stage weathering of fresh mineral surfaces. *American Mineralogist*, *55*(11–12), 2076–2094.

Kale, V. S. (2009). The Western Ghat: The Great Escarpment of India. In P. Migon (Ed.), *Geomorphological Landscapes of the World* (pp. 257–264). Springer Netherlands. https://doi.org/10.1007/978-90-481-3055-9_26

Keeney, D. R. (2015). Principles of Microbial Processes of Chemical Degradation, Assimilation, and Accumulation. In D. W. Nelson, D. E. Elrick, & K. K. Tanji (Eds.), *SSSA Special Publications* (pp. 153–164). Soil Science Society of America and American Society of Agronomy. https://doi.org/10.2136/sssaspecpub11.c11

Krám, P., Hruška, J., Wenner, B. S., Discoll, C. T., & Johnson, C. E. (1997). [No title found]. *Biogeochemistry*, *37*(2), 173–202. https://doi.org/10.1023/A:1005742418304

Likens, G. E. (1997). *Biogeochemistry of a forested ecosystem*. Springer.

Mackay, J. R. (1993). Air temperature, snow cover, creep of frozen ground, and the time of ice-wedge cracking, western Arctic coast. *Canadian Journal of Earth Sciences*, *30*(8), 1720–1729. https://doi.org/10.1139/e93-151

MANLEY, E. P., & EVANS, L. J. (1986). DISSOLUTION OF FELDSPARS BY LOW-MOLECULAR-WEIGHT ALIPHATIC AND AROMATIC ACIDS. *Soil Science*, *141*(2). https://journals.lww.com/soilsci/fulltext/1986/02000/dissolution_of_feldspars_by_low_molecular_weight.2.aspx

Mackenzie, F. T., & Garrels, R. M. (1971). *Evolution of sedimentary rocks*. New York: Norton.

Melluso, L., & Sethna, S. F. (2011). Mineral Compositions in the Deccan Igneous Rocks of India: An Overview. In J. Ray, G. Sen, & B. Ghosh (Eds.), *Topics in Igneous Petrology* (pp. 135–159). Springer Netherlands. https://doi.org/10.1007/978-90-481-9600-5_7

Meybeck, M. (1987). Global chemical weathering of surficial rocks estimated from river dissolved loads. *American journal of science*, *287*(5), 401–428.

Millot, R., Gaillardet, J., Dupré, B., & Allègre, C. J. (2002). The global control of silicate weathering rates and the coupling with physical erosion: New insights from rivers of the Canadian Shield. *Earth and Planetary Science Letters*, *196*(1–2), 83–98. https://doi.org/10.1016/S0012-821X(01)00599-4

Mooley, D. A., Parthasarathy, B., Sontakke, N. A., & Munot, A. A. (1981). Annual rain- water over India, its variability and impact on the economy. *Journal of Climatology*, *1*(2), 167–186. https://doi.org/10.1002/joc.3370010206

Myneni, R. B., Hall, F. G., Sellers, P. J., & Marshak, A. L. (1995). The interpretation of spectral vegetation indexes. *IEEE Transactions on Geoscience and Remote Sensing*, *33*(2), 481–486. https://doi.org/10.1109/TGRS.1995.8746029

Nesbitt, H. W., & Wilson, R. E. (1992). Recent chemical weathering of basalts. *American Journal of Science*, *292*(10), 740–777. https://doi.org/10.2475/ajs.292.10.740

Newton, R. C. (1992). An overview of charnockite. *Precambrian Research*, *55*(1–4), 399–405. https://doi.org/10.1016/0301-9268(92)90036-N

Oliva, P., Viers, J., & Dupré, B. (2003). Chemical weathering in granitic environments. *Chemical Geology*, *202*(3–4), 225–256. https://doi.org/10.1016/j.chemgeo.2002.08.001

Pichamuthu, C. S. (1969). Nomenclature of charnockites. *Indian Mineralogist*, *10*, 23-35. https://books.google.co.in/books?id=16PkAAAAMAAJ

Pullaiah, T. (Ed.). (2024). *Biodiversity hotspot of the Western Ghats and Sri Lanka* (First edition). AAP/Apple Academic Press.

Rajesh, H. M., & Santosh, M. (2012). Charnockites and charnockites. *Geoscience Frontiers*, *3*(6), 737–744. https://doi.org/10.1016/j.gsf.2012.07.001

Rao, Y. P. (1976). *Southwest Monsoon*. India Meteorological Department. https://books.google.co.in/books?id=16PkAAAAMAAJ

Running, S. W. (1990). Estimating Terrestrial Primary Productivity by Combining Remote Sensing and Ecosystem Simulation. In R. J. Hobbs & H. A. Mooney (Eds.), *Remote Sensing of Biosphere Functioning* (Vol. 79, pp. 65–86). Springer New York. https://doi.org/10.1007/978-1-4612-3302-2_4

Sak, P. B., Fisher, D. M., Gardner, T. W., Murphy, K., & Brantley, S. L. (2004). Rates of weathering rind formation on Costa Rican basalt 1 1Associate editor: E. H. Oelkers. *Geochimica et Cosmochimica Acta*, *68*(7), 1453–1472. https://doi.org/10.1016/j.gca.2003.09.007

Sieffermann, G., & Millot, G. (1969). *Equatorial and tropical weathering of recent basalts from Cameroon: Allophanes, halloysite, metahalloysite, kaolinite and gibbsite. (Vol. 1, pp. 417-430)*, 417–430.

Stallard, R. F. (1985). River Chemistry, Geology, Geomorphology, and Soils in the Amazon and Orinoco Basins. In J. I. Drever (Ed.), *The Chemistry of Weathering* (pp. 293–316). Springer Netherlands. https://doi.org/10.1007/978-94-009-5333-8_17

Stumm, W. (Ed.). (1967). *Equilibrium Concepts in Natural Water Systems* (Vol. 67). AMERICAN CHEMICAL SOCIETY. https://doi.org/10.1021/ba-1967-0067

Subramanian, A. P. (1959). Charnockites of the type area near Madras; a reinterpretation. *American Journal of Science*, *257*(5), 321-353.

Washington, H. S. (1922). Deccan traps and other plateau basalts. *Geological Society of America Bulletin*, *33*(4), 765–804. https://doi.org/10.1130/GSAB-33-765

West, A., Galy, A., & Bickle, M. (2005). Tectonic and climatic controls on silicate weathering. *Earth and Planetary Science Letters*, *235*(1–2), 211–228. https://doi.org/10.1016/j.epsl.2005.03.020

White, A. F., & Blum, A. E. (1995). Effects of climate on chemical_ weathering in watersheds. *Geochimica et Cosmochimica Acta*, *59*(9), 1729–1747. https://doi.org/10.1016/0016-7037(95)00078-E

White, A. F., Blum, A. E., Bullen, T. D., Vivit, D. V., Schulz, M., & Fitzpatrick, J. (1999). The effect of temperature on experimental and natural chemical weathering rates of granitoid rocks. *Geochimica et Cosmochimica Acta*, *63*(19–20), 3277–3291. https://doi.org/10.1016/S0016-7037(99)00250-1